Paleoceanography and Paleoclimatology

RESEARCH ARTICLE
10.1029/2018PA003413

PRYSM v2.0: A Proxy System Model for Lacustrine Archives

Sylvia G. Dee[1,2,3], James M. Russell[1,2], Carrie Morrill[4,5], Zihan Chen[1], and Ashling Neary[1]

[1]Department of Earth, Environmental, and Planetary Sciences, Brown University, Providence, RI, USA, [2]Institute at Brown for Environment and Society, Brown University, Providence, RI, USA, [3]Department of Earth, Environmental, and Planetary Sciences, Rice University, Houston, TX, USA, [4]Cooperative Institute for Research in Environmental Sciences, University of Colorado Boulder, Boulder, CO, USA, [5]NOAA's National Centers for Environmental Information, Boulder, CO, USA

Abstract Reconstructions of temperature and hydrology from lake sedimentary archives have made fundamental contributions to our understanding of past, present, and future climate and help evaluate general circulation models (GCMs). However, because paleoclimate observations are an indirect (proxy) constraint on climatic variables, confounding effects of proxy processes complicate interpretations of these archives. To circumvent these uncertainties inherent to paleoclimate data-model comparison, proxy system models (PSMs) provide transfer functions between climate variables and the proxy. We here present a new PSM for lacustrine sedimentary archives. The model simulates lake energy and water balance, sensors including leaf wax δD and carbonate $\delta^{18}O$, bioturbation, and compaction of sediment to lend insight toward how these processes affect and potentially obfuscate the original climate signal. The final product integrates existing and new models to yield a comprehensive, modular, adaptable, and publicly available PSM for lake systems. Highlighting applications of the PSM, we forward model lake variables with GCM simulations of the last glacial maximum and the modern. The simulations are evaluated with a focus on sensitivity of lake surface temperature and mixing to climate forcing, using Lakes Tanganyika and Malawi as case studies. The PSM highlights the importance of mixing on interpretations of air temperature reconstructions from lake archives and demonstrates how changes in mixing depth alone may induce nonstationarity between in situ lake and air temperatures. By placing GCM output in the same reference frame as lake paleoclimate archives, we aim to improve interpretations of past changes in terrestrial temperatures and water cycling.

Plain Language Summary Paleoclimate data from lakes provide some of the richest records of past changes in temperature and precipitation on Earth. Indeed, the wealth of data from and global coverage of large lake systems makes these records a particularly apt target for testing the performance of global climate models. However, comparing models to lake archives is nontrivial: the two data types are starkly different, and a model is required to "translate" between them. This paper builds a framework for modeling lakes that places climate model and paleoclimate proxy measurements in the same units by accounting for all the ways in which the climate signal of interest (e.g., temperature) is modified by the lake (e.g., the heat budget of the lake or sedimentation processes). By making more direct comparisons between data and models, we hope to build connections between researchers working with climate models and researchers who produce lake records of past climate. In general, our lake model helps the climate science community interpret the drivers of past climate changes from lakes. These records from the past give us context for how the climate system may respond to anthropogenic greenhouse gas forcing in the future.

Key Points:
- We present a publicly available forward model for lake paleoclimate archives, expanding open-source tools for PRoxY System Modeling (PRYSM)
- The model simulates lake energy and water balance, sensors including TEX_{86}, leaf wax δD, and carbonate $\delta^{18}O$, bioturbation, and compaction
- Modeling the full lake system demonstrates importance of mixing, nonstationarity, and seasonality in lake paleoclimate archives

Supporting Information:
- Supporting Information S1

Correspondence to:
S. G. Dee,
sylvia.dee@rice.edu

Citation:
Dee, S. G., Russell, J. M., Morrill, C., Chen, Z., & Neary, A. (2018). PRYSM v2.0: A proxy system model for lacustrine archives. *Paleoceanography and Paleoclimatology*, *33*, 1250–1269. https://doi.org/10.1029/2018PA003413

Received 5 JUN 2018
Accepted 1 OCT 2018
Accepted article online 5 OCT 2018
Published online 23 NOV 2018

1. Introduction

Lake sedimentary archives have yielded some of the most complete, time-continuous records of terrestrial climate changes and have provided fundamentally important observations of thermal and hydrological change extending centuries to millennia into the past. Efforts to amass paleoclimate reconstructions from lake sediments have provided regionally coherent understanding of temperature variability and paleohydrology from the last glacial maximum (LGM) to the present (c.f. Gasse, 2000; Harrison et al., 2016; Street-Perrott, 1994), and these records serve as an important test bed for climate model simulations (e.g., Kutzbach & Street-Perrott, 1985; Loomis et al., 2017; Otto-Bliesner et al., 2014). Recently, considerable attention has been cast toward data-model comparison, and in particular evaluating the ability of coupled general circulation models (GCMs) to simulate the variability observed in proxy archives (e.g., Dee et al., 2017; Laepple & Huybers, 2014). Such

work harbors implications for the limitations of climate model physics, in particular the ability of Intergovernmental Panel on Climate Change (IPCC)-class GCMs to capture decadal to centennial variability of the atmospheric and terrestrial water cycle in future climate simulations (IPCC, 2013, and references therein).

In general, making robust comparisons between complex, multivariate paleoclimate archives (including lacustrine archives) and climate model simulations is not straightforward. Traditionally, paleoclimate reconstruction techniques for lakes have employed empirical (and usually linear) calibrations between proxy measurements and the climate variable of interest (e.g., Loomis et al., 2011, 2012; Powers et al., 2011, and many others). This *inverse modeling* approach accounts for calibration uncertainties but incurs errors in assuming stationarity of those calibrations and the linearity of the proxy's response to climate forcing. There is thus a growing need for new methods in data-model comparison that take into account the differences between climate models, which generate climate fields such as temperature, precipitation, and wind speed, and paleoclimate archives, which may record a multivariate, seasonally biased, and biologically, geochemically, and geologically influenced transformation of the input climate signal. Complementary to the inverse modeling approach, *forward* models predict the proxy value from climate variables using a first-principles representation of how the proxy works. A forward model or proxy system model (PSM; Evans et al., 2013) incorporates our understanding of the physical, chemical, geological, and biological processes that affect the paleoclimate archive we measure (Baker et al., 2012; Evans et al., 2013; Russon et al., 2013; Schmidt, 1999; Stoll et al., 2012; Thompson et al., 2011; Wackerbarth et al., 2012; and see Dee et al., 2015, for a review). Generally, a paleoclimate archive's encoding of climate forcing may manifest as a multivariate and nonlinear signal (Dee et al., 2015).

PSMs for multiple proxy types have been published in recent years, particularly for high-resolution (e.g., tree ring width) and water-isotope-based systems (ice cores, corals, tree cellulose, and speleothems; see Dee et al., 2015; Evans et al., 2013, for a review). These models have proved their usefulness, facilitating studies which expand understanding of the climate signals recorded by proxy data (Anchukaitis et al., 2006; Baker et al., 2012; Stoll et al., 2012; Wackerbarth et al., 2012), partitioning the impacts of the proxy system itself on the final measurement (Dee et al., 2015), and improving data-model comparison by placing models and paleoclimate observations in the same reference frame or in the same units (e.g., Russon et al., 2013; Steig et al., 2013; Thompson et al., 2011). Further, PSMs have been implemented in paleoclimate data assimilation (Dee et al., 2016; Steiger et al., 2014) and in tracking error contributions inherent to different proxy types (Dee et al., 2015). However, to date, there has been little attempt to develop a full PSM for lake temperature and hydroclimate proxies. Although many studies have developed forward models for sedimentary archives (e.g., Huybers & Wunsch, 2004; Jones et al., 2016; Schmidt, 1999; Subin et al., 2012; Trauth, 1998), these models have primarily focused on a single aspect of the system, for example, energy balance (Hostetler & Bartlein, 1990), sedimentation, and compaction (Bahr et al., 2001; Huybers & Wunsch, 2004; Lou et al., 2000) or bioturbation (Trauth, 2013). Each of these models is coded in different programming languages, using different conventions, and often is designed for a specific site or problem, and they are thus not readily adaptable for wider use. Standard frameworks for the design of these models are needed to encourage broader use in the paleoclimate community.

To address this, we here describe the design and application of a new Lake Sedimentary Archive PSM to translate climate model output and observations to lake temperature observations from proxy data. Our goal is to provide a flexible, multifaceted lake model that can be adapted depending on the user's research question. The model is broadly applicable to a range of scientific questions in paleolimnology; for example, one can to perform sensitivity tests for controls on lake surface temperature, mixing depth, and lake level. Previous work has used components of the lake PSM to simulate lake level, indicative of changes in the hydrological cycle (Hostetler, 2009; Hostetler & Benson, 1994; Li & Morrill, 2013; Lowry & Morrill, 2018); in this study, we focus on how lake temperatures are encoded in a proxy measurement and the uncertainties imparted on that measurement during sedimentation and bioturbation, for example. An important application of the new lake PSM is its use in data-model comparison. Comparing lake temperature reconstructions to climate model output helps highlight discrepancies in our understanding of both climate physics and proxy uncertainties. The lake PSM further provides a point of contact between the climate modeling community and the lacustrine archive community.

We apply the PSM to Lakes Tanganyika and Malawi, using time-slice experiments from the Paleoclimate Modeling Intercomparison Project (PMIP3) to simulate lake temperature changes under different mean climate

states. We use the PSM output to (1) evaluate the energy and mass transfers that drive simulated lake temperature changes, (2) evaluate proxy biases, (3) and test whether simulated lake surface temperature changes (the variable commonly reconstructed by proxies) track simulated air temperature changes. We find that the PSM simulations highlight the importance of mixing in our interpretations of absolute temperature changes in the past.

The Lake Sedimentary Archive PSM is built into existing, publicly available software in Python, PRoxy sYStem Modeling (PRYSM), a framework for the design and user contribution of PSMs. The model constitutes an open-source, comprehensive, globally applicable lake sedimentary archive PSM. The final product is distributed through Github (https://github.com/sylvia-dee/PRYSM). We introduce the concept of PSMs and describe the details of our implementation of each of the Lake PSM's submodels in section 2. To demonstrate the viability of our approach, we apply the forward model to output from PMIP3 climate model simulations at Lakes Tanganyika and Malawi in section 3, investigating uncertainties related to temperature reconstructions and mixing depths during the LGM. We evaluate temperature changes in reconstructions and coupled climate models, the relationship between lake and air temperatures via proxy system modeling, and the accuracy of numerical model predictions of past African temperature changes. Finally, we discuss the relevance of our findings for broad application in the paleoclimate community, caveats, and extensions of this work in section 4.

2. Proxy System Modeling for Lacustrine Archives of Past Climate

Climate observations in lake sediments are influenced by multiple climatic variables including (but not limited to) temperature, precipitation, humidity, wind speed, radiation at the surface, and the seasonality of these variables. The multivariate nature of the climatic forcings on lake sedimentary archives necessitates transfer models which simulate both the input climate and the processes that govern the proxy's recording of that climate signal. These transfer models, called PSMs, convert GCM simulations to pseudoproxy records, and are now considered a fundamental step for robust data-model comparison (Dee et al., 2015; Harrison et al., 2015).

Our design of the lake PSM follows previous work (Dee et al., 2015; Evans et al., 2013) dividing the full model into four main components of the proxy system response to climate forcing. Each component simulates a separate modification of the primary climate signal as it is embedded in a proxy. First, an *Environment Model* accounts for the impacts of the regional or local climatic drivers at the proxy measurement site; for lakes in particular, this includes the energy balance and hydrology of the lake system. The *Sensor Model* describes the physical, geochemical, and/or biological response of the proxy to the environment climate forcing, and the *Archive Model* describes the emplacement or deposition of the *sensor's* response to the environmental forcing (in a layer of sediment or ice, for example). Finally, the *Observation Model* describes how measurements are made on the archive and accounts for errors in dating/chronology, sampling, replication, and various analytical uncertainties. Following this framework, we extend PRYSM1.0 (Dee et al., 2015) with the addition of a PSM for lacustrine sediments, branding the extension PRYSM2.0. The full PSM uses a lake energy and water balance model to drive the sensor, archive, and observation submodels in succession, described below. Finally, the lake model uses Python, a widely used and supported open-source programming language in climate data analysis and visualization. The full PSM produces GCM-simulated climate variables translated to *proxy units* (e.g., $\delta^{18}O_{CARBONATE}$, δD_{WAX}, and glycerol dialkyl glycerol tetraether [GDGT]) for direct comparison to the measured temperature and hydroclimate records.

2.1. *Environment*: Hydrological, Isotopic and Energy Balance Submodel

The environment component of this PSM is a one-dimensional lake thermal and hydrological model originally developed by Hostetler and Bartlein (1990, which gives full documentation). Hostetler (1991) incorporated the more sophisticated lake ice model of Patterson and Hamblin (1988), and Hostetler and Benson (1994) added the isotopic module. Small et al. (1999) made modifications to improve the ice model and other components, including new parameterizations for sensible and latent heat flux from the Biosphere-Atmosphere Transfer Scheme land surface model, a Crank-Nicholson numerical solution to improve simulation of temperature changes by eddy diffusion, inclusion of the effects of salinity on water properties and evaporation, and implementation of a partial ice cover scheme. Lastly, Morrill et al. (2001) added subroutines to allow sigma-level atmospheric model data as input. In our implementation, we additionally allow the user to specify the neutral drag coefficient, depth-varying salinity, and albedos for melting and nonmelting snow to provide more flexibility in lake-specific applications.

The lake model requires seven input variables from either meteorological observations, reanalysis products, or GCMs: near-surface air temperature, near-surface specific humidity, downward shortwave radiation, downward longwave radiation, near-surface wind speed, precipitation, and surface pressure. For these variables, the current model configuration uses monthly mean input data, but previous versions have been run with daily or 6-hourly inputs, and the model time-step can be adapted depending on the user's research needs. The relative or specific humidity (q) is used to calculate the specific humidity gradient from lake surface to surface air, which impacts the rate of evaporation. Runoff amounts are needed if the user wishes to simulate water balance (i.e., lake levels over time). A full description of the lake level module is given in Hostetler and Benson (1994) and Hostetler (2009), and it has been successfully applied across a wide range of climatic regimes (Li & Morrill, 2013; Lowry & Morrill, 2018; Small et al., 1999; Vassiljev et al., 1998).

Runoff values may be obtained in a variety of different ways, including from observations (Hostetler, 2009), full catchment streamflow models (e.g., Barth et al., 2016; Matsubara & Howard, 2009), and Budyko (1961) or other rainfall-runoff scaling assumptions (Ibarra et al., 2018; Quade et al., 2018; Steinman et al., 2013). It is also possible to use simulated lake evaporation from the environment model in conjunction with qualitative runoff estimates to produce qualitative lake level information (Li & Morrill, 2013; Lowry & Morrill, 2018).

The water isotope balance module of the model requires inputs of isotope ratios ($\delta^{18}O, \delta D$) in precipitation and runoff. These values may be taken from an isotope-enabled model or observations, when available (e.g., WaterIsotopes.org; Bowen, 2009), or run using a simple site-specific calibration with temperature (see READ.me; supporting information S1). The isotopic water balance scheme in the lake model is outlined in Benson (1994), Hostetler and Benson (1994), and Benson and White (1994), with updates in the current version of the model specific to Lake Tanganyika. Importantly, the water isotope ratios of the surface lake water are used as inputs to the $\delta^{18}O$ of carbonate sensor model, described in section 2.2. The isotope-enabled model inputs used for this iteration of the lake model are described in supporting information S1.

With the exception of the water isotope ratios and potential catchment data, the climatological input variables needed to run the lake environment model are readily available in reanalysis data (e.g., National Centers for Environmental Prediction or ERA-Interim) and for nearly all of the Climate and Paleoclimate Model Intercomparison Project 3 (PMIP3) simulations at monthly resolution. A full list of inputs and outputs for the Environment submodel is given in Table S1.

The environment model then calculates standard outputs from the surface energy balance, wind-driven turbulent mixing using an eddy diffusion scheme, and density-driven convective mixing (Figure 1). Two output files are generated from the model, `surface.dat` and `profile.dat`. The `READ.ME` (supporting information S1) file details the content of these outputs (section S2.1), which in the current configuration include lake surface temperature, mixing depth, evaporation, and water isotope ratios in the surface water.

We note that some lake-specific tuning of the environment model parameters may be necessary. A full step-by-step guide for tuning the model for a given lake site, as well as justification for our parameter choices for lake Tanganyika, can be found in section S4. In general, values for lake-specific parameters (e.g., depth, salinity, and shortwave extinction coefficient) should be set using modern observations as much as possible. Finally, given the necessity of de-biasing GCM output, we also employed the commonly used delta method to generate climate inputs for paleo PSM simulations, which involves scaling modern observations or reanalysis data by the paleo to modern change (δ) simulated by the GCM (e.g., Lorenz et al., 2016).

2.2. *Sensor*: Proxy Measurements in Lake Sediments

Lake sediments, like other paleoclimate archives, may commingle multiple sensors within one archive. Observations from lake sediments may include, but are not limited to, $\delta^{18}O_{CARBONATE}$, biomarkers and their isotopes, GDGTs, lake level, diatoms, chironomids, ostracods, pollen, lithologic/geochemical measurements (varve thickness, sediment composition, and carbonate precipitation), isotope ratios of carbon and nitrogen, isotope ratios of bulk organic matter, tephras, and elemental abundances.

Focusing on primary climate variables (i.e., temperature and precipitation), historically, paleoecological proxies such as pollen and chironomids have dominated this field, but newly developed proxies for air temperature from lake sediments have employed organic and inorganic geochemical temperature proxies based upon GDGTs including TEX_{86} and brGDGTs (Kraemer et al., 2015; Loomis et al., 2011, 2012; Powers et al., 2011; Tierney et al., 2008; Tierney, Oppo, et al., 2010; Tierney & Tingley, 2015). Oxygen isotopes in carbonates ($\delta^{18}O_{CARB}$) have been used to reconstruct both lake water temperature and water balance, while others have

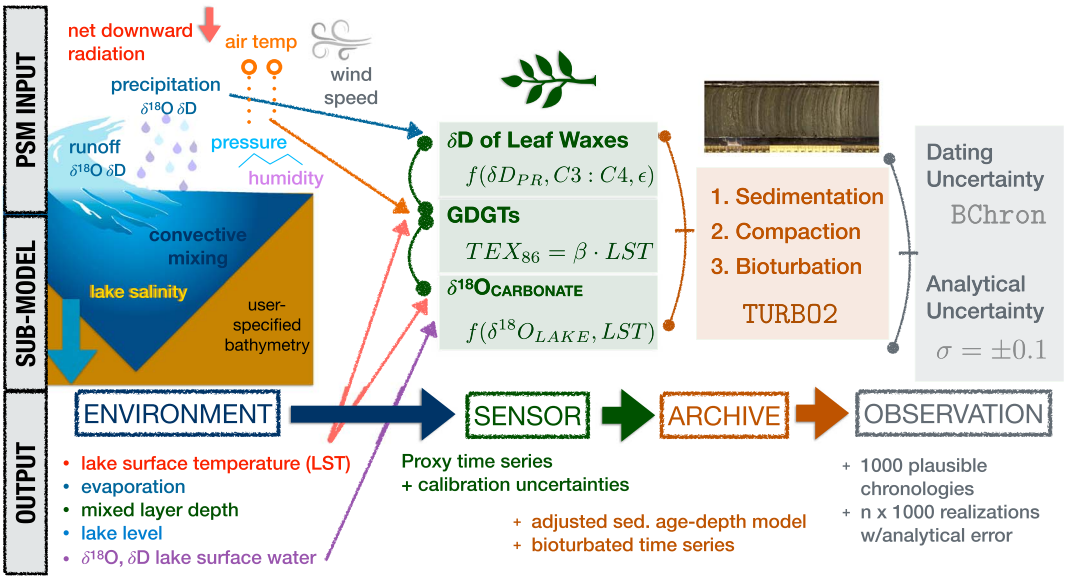

Figure 1. Full Lake PSM Schematic. The lake PSM is composed of four submodels: *environment*, *sensor*, *archive*, and *observation*, all of which utilize/produce unique inputs/outputs. The figure shows the components of the Lake PSM, which is adaptable and modular by design to facilitate additions and modifications to any of the submodels included in this version. Model inputs and outputs for the full lake PSM are given in Table S1. PSM = proxy system model; GDGT = glycerol dialkyl glycerol tetraether.

measured proxies generally considered sensitive to precipitation amount such as the hydrogen isotopic composition of leaf waxes (δD_{WAX}; Costa et al., 2014; Feakins et al., 2014; Konecky et al., 2011; Russell et al., 2009, 2014; Tierney, Russell, & Huang, 2010). It is possible to build any number of sensor models appropriate for inclusion in a comprehensive lake PSM. However, for this release of `PRYSM2.0`, we have included just three: GDGTs, δD_{WAX}, and $\delta^{18}O_{CARB}$. We plan to continue extending the sensor model's functionality and readily welcome additional contributions. We briefly describe each of the currently available sensor models here:

1. δD_{WAX}

   Lacustrine sediments capture and preserve epicuticular plant waxes (δD_{wax}), from which the hydrogen isotopic composition (D/H) can be extracted. These hydrogen isotope ratios are widely used to reconstruct past changes in both temperature and hydroclimate (Sachse et al., 2012 and references therein). These isotope ratios are derived from hydrogen supply available for biosynthesis of plant wax compounds; these include long-chain *n*-alkanes, *n*-alkanoic acids, and *n*-alkanols. The hydrogen supply itself is derived from environmental water used by plants during growth. The leaf wax hydrogen isotope ratios capture the δD of the source water, which depends on changes in local and regional hydroclimate (e.g., precipitation amount or source). As a result, these proxies have been employed to reconstruct past changes in the global hydrological cycle.

   The sensor model is designed based on the theory presented in Sachse et al. (2012) and expanded in Konecky et al. (2016) and accounts for plant-specific impacts such as differences between photosynthetic pathway and leaf evaporation on biosynthetic fractionation. We specify an apparent biological fractionation (ϵ) between the input δD_{WATER} and δD_{WAX}, following the methodology presented in Konecky et al. (2016). δD ratios for the C_{29} *n*-alkane are subsequently calculated via precipitation δD time series, included in the input files accompanying this model, and the corresponding apparent fractionation values (ϵ):

$$\epsilon_{WAX-P_{veg}} = (fC_3 \cdot \epsilon_{C27.alk-P_{C3}}) + (fC_4 \cdot \epsilon_{C27.alk-P_{C4}}), \quad (1)$$

where fC_3 and fC_4 are the fractions of C_3 and C_4 plants, respectively, and $\epsilon_{C27.alk-P_C3}$ and $\epsilon_{C27.alk-P_C4}$ are average apparent fractionation factors ϵ_{WAX-P} for the C27 *n*-alkane, and $\epsilon_{alkane-acid}$ is the average alkane-acid

offset observed between C28 *n*-acid and C27 *n*-alkane in *n*-alkane biosynthesis (Konecky et al., 2016; Sachse et al., 2012). Biological fractionation factors are subsampled from a distribution built based on observations reported in Sachse et al. (2012), where $\epsilon_{C27.alk-P_C3} = -112.8 \pm 34.7‰$ and $\epsilon_{C27.alk-P_C4} = -124.5 \pm 28.2‰$; these values represent the global average of ϵ_{C29} measurements from all plant groups (Sachse et al., 2012). A predicted value for δD_{WAX} is then calculated by inverting equation (2) from Konecky et al. (2016) using δD_{PRECIP} as an input:

$$\delta D_{WAX} = (\delta D_{PRECIP} + 1,000) \cdot (\epsilon_{WAX-P_{veg}}/1,000 + 1.0) - 1,000. \quad (2)$$

To use the δD_{WAX} sensor model, inputs from a water isotope-enabled atmospheric model to simulate water isotope ratios in precipitation and soil water (if available) are required. If in situ measurements of precipitation isotopes are available (e.g., a proximal station of the Global Network of Isotopes in Precipitation; IAEA/WMO, 2014), such inputs may also be used for a given lake site. The example input files published alongside this work include monthly time series of δD_{PRECIP} from the isotope-enabled atmospheric model iCAM5 (Nusbaumer et al., 2017) over Tanganika.

This sensor model in its current configuration employs fixed values for ϵ_{WAX-P}; while this configuration allows us to predict variations in δD_{WAX} resulting from changes in water isotopes in precipitation (δD_{precip}) alone, it assumes that vegetation composition remains constant over time, which is not wholly realistic. More complex leaf wax sensor models which take into account differences between vegetation types and ϵ values for each plant functional type based on global vegetation distributions, as well as changes in land cover over time, are forthcoming and will be incorporated into this version of `PRYSM v2.0` upon publication.

2. $\delta^{18}O_{CARB}$

Many lake archives provide long, continuous records of past oxygen isotope ratios ($\delta^{18}O$), and these records have been collected with considerable global coverage (Viau & Gajewski, 2001). Oxygen isotopes can be measured in a number of proxy media including diatoms and cellulose but especially in carbonates such as ostrocods, gastropods, and bulk sedimentary carbonates ($\delta^{18}O_{CARB}$). $\delta^{18}O_{CARB}$ varies as a function of lake water temperature and isotope ratios (Dean et al., 2018; Jones et al., 2005), yielding insight to changes in both local air temperatures and the hydrological cycle (e.g., balance of precipitation minus evaporation) over time (Jones et al., 2005; Leng & Marshall, 2004). Through the use of an isotope mass balance model such as the scheme employed in the *enviroment* submodel, the specific thermodynamic versus hydrological controls on the $\delta^{18}O_{CARB}$ can be better diagnosed.

The $\delta^{18}O_{CARB}$ in lake surface water can be modeled as a function of the isotope ratios in lake water and temperature-dependent fractionation, which depends on the calcium carbonate type precipitated. The carbonate isotope sensor model directly computes the proxy observation ($\delta^{18}O_{CARB}$) from the output of the environment model: simulated water isotopes and temperature. The transfer function for $\delta^{18}O_{CARB}$ can be modified by the user and includes the unit conversion from Vienna Pee Dee Belemnite to Vienna Standard Mean Ocean Water, as well as the temperature-dependent fractionation between $\delta^{18}O_{WATER}$ and carbonate:

$$\delta^{18}O_{CARB} = \delta w + 21.9 - \sqrt{21.9 \cdot 21.9 - 10 \cdot (16.9 - T)} \quad (3)$$

$$\delta w = \delta^{18}O_w - 0.2, \quad (4)$$

(O'Neil et al., 1969),

$$\delta^{18}O_{CARB} = \delta w + 25.8 - \sqrt{25.8 \cdot 25.8 - 11.1 \cdot (16.1 - T)} \quad (5)$$

$$\delta w = \delta^{18}O_w - 0.27, \quad (6)$$

(Kim & O'Neil, 1997),

$$\delta^{18}O_{CARB} = \delta w + 25.8 - \sqrt{25.8 \cdot 25.8 - 11.1 \cdot (16.1 - T)} \quad (7)$$

$$\delta w = \delta^{18}O_w - 0.22, \quad (8)$$

(Erez & Luz, 1983),

$$\delta^{18}O_{CARB} = \delta w + (13.2 - T)/4.89 \quad (9)$$

$$\delta w = \delta^{18}O_w - 0.27, \quad (10)$$

(Bemis et al., 1998),
where T is lake surface temperature, δw is the Vienna Standard Mean Ocean Water correction for $\delta^{18}O_{WATER}$, and $\delta^{18}O_w$ is the oxygen isotope composition of the surface lake water.
Importantly, the $\delta^{18}O_{CARB}$ sensor model should only be used in the current version of the PSM framework if the water balance and isotope mass balance modules of the environment model are turned on to properly model $\delta^{18}O_{LAKE}$.

3. TEX_{86} and (br)GDGT
The sensor model includes transfer functions for TEX_{86} or the TetraEther indeX of 86 carbons proxy for marine and lacustrine temperatures. TEX_{86} is used as a proxy for marine and lacustrine temperatures. It is defined to quantify the degree of cyclization of isoprenoidal GDGTs (iso-GDGTs) produced by Archaea (Schouten et al., 2002). Second, branched GDGTs (brGDGTs) are produced by bacteria and are preserved in a range of natural archives. Weijers et al. (2007) was first to show their degree of cyclization and methylation (quantified by the Methylation of Branched Tetraether – MBT – and the Cyclisation of Branched Tetraether – CBT – indices, respectively) correlate to temperature in soils. More recently, these compounds have been shown to capture changes in mean annual air temperatures (MAAT) based on changes in the fractional abundances of a set of 14 brGDGTs (De Jonge et al., 2014; Russell et al., 2018).
The sensor model acquires temperatures at different depths and seasons from the environment model and treats these temperatures as a proxy signal. If a direct transfer function relating temperature to GDGTs is available for a given site or region, it can be specified as the parameter β in function `lake_sensor_gdgt.py`. For the purposes of demonstration, a number of potential calibration values for β are listed based on values used by Powers et al. (2011) and Loomis et al. (2017).
The temperature-TEX_{86} relationship is inverted to yield a forward estimate of the proxy measurement:

$$TEX_{86} = \beta * LST, \quad (11)$$

$$TEX_{86} = (LST + 14.0)/55.0, \text{ [Powers et al., 2011]} \quad (12)$$

$$TEX_{86} = (LST + 10.92)/54.88, \text{ [Loomis et al., 2017]} \quad (13)$$

where LST is lake surface temperature, and β is the proxy/temperature transfer function or calibration set by the user.
Recent calibration studies have developed calibrations for brGDGTs in lakes with mean annual temperatures based upon a version of the MBT index which use only 5-methyl isomers (MBT'_{5ME}). These compounds in particular have been shown to correlate with MAAT (e.g., De Jonge et al., 2014; Russell et al., 2018).

$$MBT'_{5ME} = (MAAT + 1.21)/32.42, \text{ [Russell et al., 2018]}, \quad (14)$$

$$MBT'_{5ME} = (MAAT + 8.57)/31.45, \text{ [De Jonge et al., 2014]}. \quad (15)$$

As mentioned above, the GDGT component of the sensor model is modular such that the user may specify which calibration to use based on recent publications or can specify their own value for β. Additional calibration options will be added to the submodel as they are published. An example of the GDGT sensor model output is given in Figure 4.

2.3. *Archive* Model: Sedimentation, Bioturbation, and Compaction

The archive submodel simulates sedimentary processes that affect the emplacement of the sensors in sediments, namely, variations in sedimentation rate, accumulation, compaction (e.g., Huybers & Wunsch, 2004), and bioturbation (Trauth, 1998, 2013). These processes smooth the reconstructed climate signal (see Figure 5, orange/red line). These effects are likely small in low-resolution, centennial-scale analyses in lake sediment measurements, but the ability to quantify the effects of these uncertainties is nevertheless important, especially for high-resolution sedimentary archives. The bioturbation model is validated in section 3.1 (and see Figure 5).

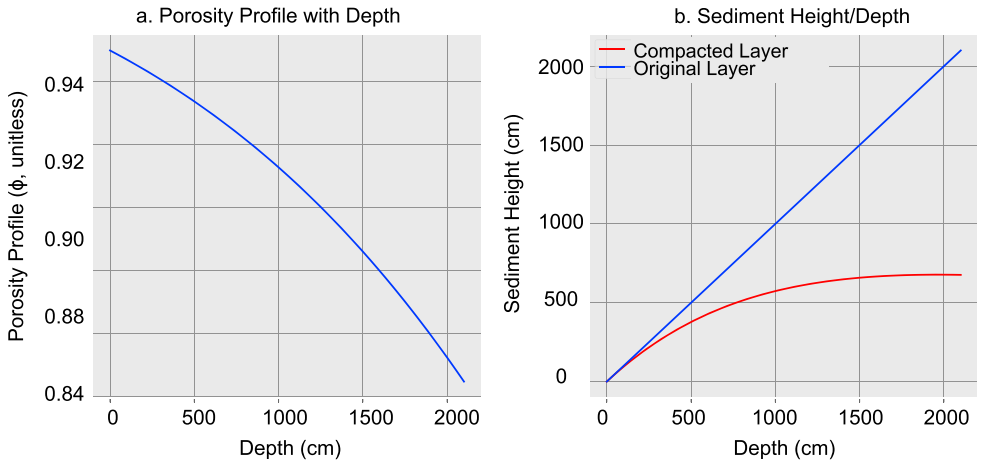

Figure 2. Sediment compaction: Porosity profile + sedimentation. The lake archive subroutine simulates sediment compaction via a simple correction for the porosity of the sediment. (a) Porosity profile in simulated sediment core spanning the last 21 kyr. (b) Original, noncompacted sediment assuming a sedimentation rate of 100 cm/kyr (blue) and compacted sediment via porosity calculation.

We model bioturbation using an adapted version of the TURBO2 parameterization described in Trauth (2013). Bioturbation and mixing in the sediment can distort the sensor proxy measurements in time. To account for this, the bioturbation module of the archive model takes the original ages, abundances, isotope or geochemical measurement (sensor model output), and number of carriers and computes a bioturbated version of the proxy data. The bioturbation model (function `lake.archive.bioturb.py`) takes four inputs, including age starting with the oldest layer, mixed layer thickness in centimeters, species abundance (for all intents and purposes, this is a constant and is set to 200 by default, and see supporting information S1 for additional information), and proxy signal (isotope, GDGT, etc.). Bioturbation effectively smoothes the input climate signal, which can reduce variance in the measured signal and alter the shape of the resulting power spectrum (Dee et al., 2015, 2017).

The sediments and the sensors within them are compacted via a correction using the porosity profile (Figure 2a). The initial porosity (ϕ) is user-specified but typically ranges from values of 0.6 to 0.99 for lake sediments (e.g., Crusius & Anderson, 1991). We calculate the porosity profile via Bahr et al. (2001):

$$\phi_z = \frac{e^{-cg(\rho_s-\rho_w)z}}{e^{-cg(\rho_s-\rho_w)z} + k1}, \tag{16}$$

where ϕ is porosity at depth z, g is gravity, $k1 = (1-\phi_0)/\phi_0$, c is an empirical constant depending on deformation, and ρ is the density of quartz (s) and water (w). The final compacted age-depth model is extracted from the porosity-corrected depth series (Figure 2b) via

$$h' = h \cdot (1-\phi_0)/(1-\phi), \tag{17}$$

where ϕ_0 is the initial porosity (0.95 in this example), h is the original sediment height-depth scale, and h' is the final compacted depth scale (red line in Figure 2. The archive model inputs include sedimentation rate, porosity of sediment, and the output of the sensor model (i.e., the pseudoproxy time series) and return a bioturbated, compacted age-depth series (Table S1).

2.4. *Observation* Model and Dating Uncertainties

Lake sediments are generally dated via chronologies anchored by radiometric or other discrete age control points, which are subsequently used to generate an age-depth relationship. The observation submodel allows us to assess the impacts of both analytical and age uncertainties, the latter of which is often generated with age assignments by tie points in these sediments. Indeed, sedimentary observations house significant age uncertainties, the confounding effects of which have been highlighted and/or modeled in previous work (e.g., Blaauw & Christen, 2011; Bronk-Ramsey, 2009; Burgess & Wright, 2003; Klauenberg et al., 2011; Parnell et al., 2011; Ramsey, 2008). Dating uncertainty is crucial for robust comparisons with GCMs or for climate reconstruction in general, and `PRYSM` incorporates a number of age modeling tools (see Dee et al., 2015).

Table 1
Comparison Between Observations From Lake Tanganyika Versus Lake Proxy System Model Simulated Conditions, Forcing the Lake Model With ERA-Interim Reanalysis Data for the Region

Climate/lake variable	Observed wet season	Modeled wet season	Observed dry season	Modeled dry season
Surface temperature (°C)	27.8 ± 0.7	28.5	25.8 ± 0.9	25.0 ± 0.7
Evaporation (mm/day)	3	4	6	4
Mixing depth (m)	50± 10	30	80±10	85

Note. Available in situ observations spanning the last few decades for Lake Tanganyika include surface temperature, evaporation, and mixing depths.

Modeling uncertainties in tie-point chronologies are necessitated by errors in our constraints on timing of events, rates of change, and stratigraphic correlations, all of which can be generated due to errors in radiocarbon calibration and interpolation (Dee et al., 2015). Many of these issues are addressed in previous work (e.g., Blaauw, 2010; Blaauw & Christen, 2011; Breitenbach et al., 2012; Bronk Ramsey, 1995; Haslett & Parnell, 2008; Parnell et al., 2011). `PRYSM` uses `Bchron` (Haslett & Parnell, 2008) to generate ensembles of chronologies, for its open-source compatibility with R and Python, and flexibility with a variety of tie-point chronologies. The full documentation for `Bchron` can be found in Haslett and Parnell (2008); briefly, it uses a Markov monotone stochastic process to generate pathways between user-input ages, the result being an ensemble of age-depth realizations. `Bchron` is also well-suited to the lake PSM as it was initially developed to assess radiocarbon (^{14}C) dating uncertainties.

Using Bchron, we explicitly simulate an ensemble of plausible age models for records including dating uncertainties. An example of the output from Bchron applied to Lake Tanganyika is discussed and validated in section 3.1 (Figure 6). The user-specified inputs for Bchron (Table S1) include the total length of core in centimeters, the age estimates at each tie point, standard error on the ages, the positions in the core, calibration curves, and an array of depth values where the user would like predicted ages in the output. Finally, Bchron requires the topmost age of the core, in years B.P. (1950 = 0 BP). The full observation model also includes proxy error from the combined analytical uncertainties in the measurement and calibration uncertainty. These analytical uncertainties are estimated through a Gaussian white noise function with user-specified analytical error (e.g., $\sigma = \pm 0.1‰$).

3. Applications: Model Validation and LGM Temperatures in African Rift Lakes

3.1. Model Validation and Tuning

We compared present-day simulations against available modern observations of temperature profiles from Lakes Malawi and Tanganyika (Descy et al., 2006; Plisnier et al., 1999), given in Table 1. Results from the simulations of both lake systems were largely comparable for LGM minus present-day conditions, so we focus our discussion here on results from Lake Tanganyika. The model was tuned to maximize agreement with available observations. For example, initial simulations of mixing depths in Lake Tanganyika forced by modern climate variables from the Paleoclimate Model Intercomparison Project (PMIP3) models (Braconnot et al., 2012; Meinshausen et al., 2011) were slightly too shallow compared to observations (O'reilly et al., 2003; Verburg & Hecky, 2003), partly due to the mixing scheme. We achieved a better fit of modeled to observed mixing depth using ERA-Interim reanalysis climate data (Dee et al., 2011) as input and by adjusting the neutral drag coefficient (CDRN), as recommended by Subin et al. (2012) for large lakes. Specifically, CDRN value was increased to a value of $2.0E-3$ to achieve reasonable dry season mixing depths and evaporation rates. For larger lakes, these higher values of CDRN are closer to those observed in the literature for land surface roughness (Garratt, 1977). The resulting simulations forced with ERA-Interim reanalysis (1979–2016; Dee et al., 2011) show strong agreement with the annual cycles of lake surface temperature, evaporation, and mixed layer depth of Lake Tanganyika (Table 1 and Figure 3).

Extending this, we applied the TEX_{86} sensor model to the output from the environment submodel for Lake Tanganyika over the modern period, 1979–2016. Figure 4 shows example output from the sensor model. The predicted TEX_{86} values are calculated via the calibration in Powers et al. (2011). For reference, the calibration error represented by the gray window in Figure 4 corresponds to a temperature error of approximately 2.5 °C (Powers et al., 2011). Note that our simulation yields an increasing trend in TEX_{86} (y axis inverted in Figure 4), in agreement with core-top observations reported in Tierney, Mayes, et al. (2010). The sensor model simulates

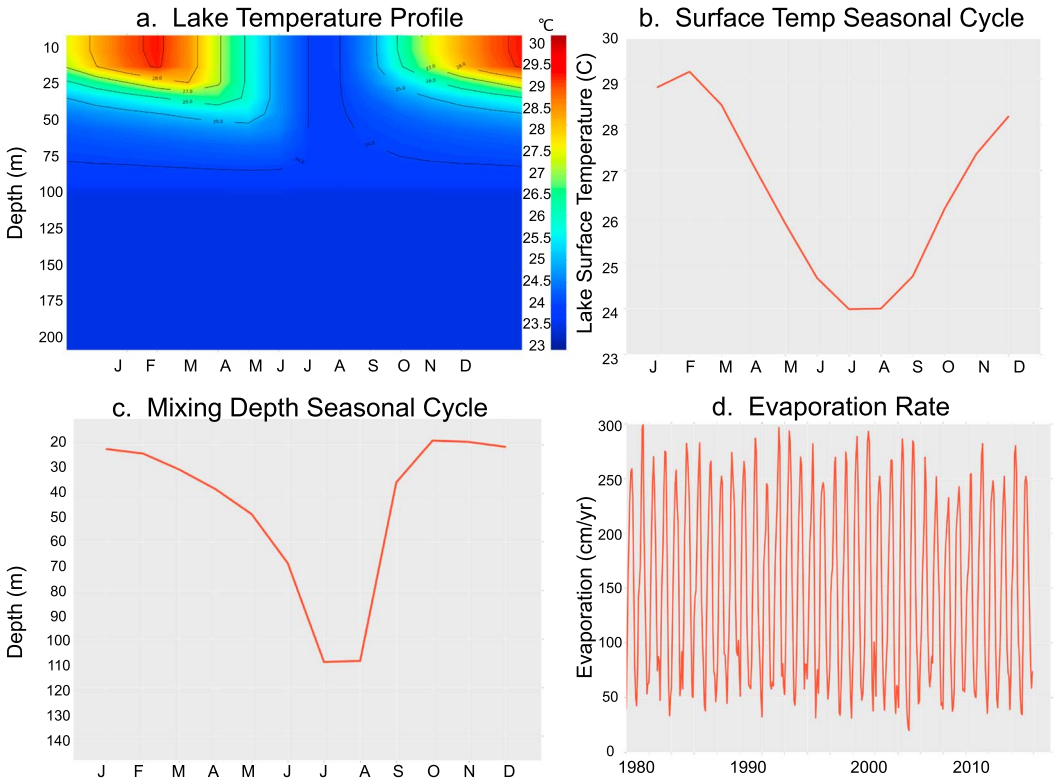

Figure 3. *Environment* model output at Lake Tanganyika using ERA-Interim Reanalysis input to the proxy system model. The lake energy balance subroutine simulates (a) temperature profile with depth, (b) seasonal cycle of lake surface temperatures, (c) mixing depth, and (d) evaporation rates (see Table 1).

TEX_{86} ranging from ~0.73 to 0.75; for reference, Tierney, Mayes, et al. (2010) report TEX_{86} values of 0.733, 0.749, and 0.752 in 1976, 1986, and 1996, respectively, using the Powers et al. (2010) calibration for Lake Tanganyika. Robust agreement between the the PSM-simulated proxy data and modern observations confirms the lake energy balance model faithfully simulates lake surface water temperatures.

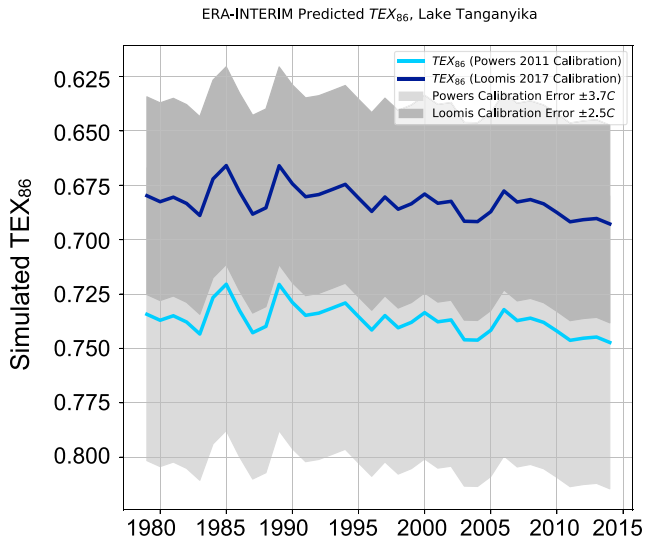

Figure 4. *Sensor* model output. TEX_{86} predicted from lake surface temperatures, using the inverted calibrations given in Powers et al. (2011) and Loomis et al. (2017; light blue and navy, respectively), with reported calibration errors. The environment model is driven with ERA-interim reanalysis data spanning 1980–2015.

The lake PSM sensor model is useful for identifying individual proxy biases. For example, the sensor model can be driven using temperature changes throughout the lake water column and across different seasons (e.g., these variables can be used as inputs from the environment model). Temperatures at specific depths or during specific seasons may best fit the observational data, isolating potential proxy system biases.

For demonstration of the bioturbation component of the lake archive submodel, Figure 5 shows the original TEX_{86} output from the lake sensor model with two possible realizations of the time series given a 4-cm-mixed layer width in the sediment. The figure highlights two important features of the signal loss imparted by the bioturbation scheme: (1) bioturbation tends to reduce the variance from the original predicted TEX_{86}, smoothing the original climate input signal, and (2) the bioturbated signal may shift peaks in the original data time series, creating errors in interpretation of absolute maxima/minima in the measured proxy signal. Examining Figure 5, the realizations from TURBO2 in red and yellow shift the local maxima of the original data occurring in 1985 and 1989 by 1–2 years. For deeper bioturbation length scales, that is, if bioturbation typically

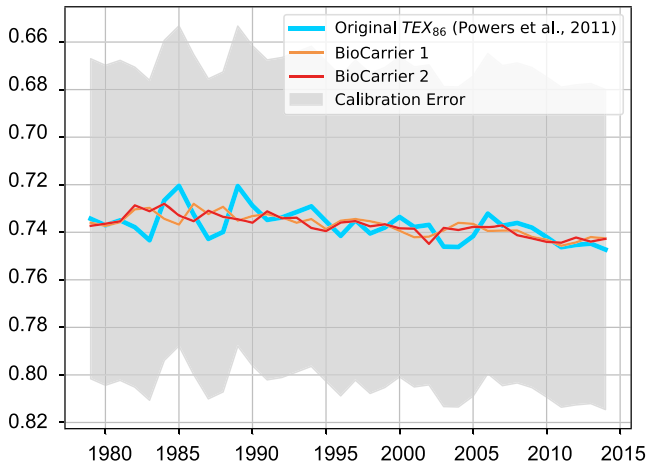

Figure 5. *Archive* validation. Simulated bioturbation of sensors (TEX_{86} in this case) using TURBO2 in Python. The figure shows TEX_{86} in Carriers 1 + 2, 4.0-cm-mixed layer, with 10 carriers. Bioturbated time series for two different elemental abundances/carriers (red, orange lines) with original (blue) with the TEX_{86} calibration error included (grey-shaded window).

occurs in the sediment over 20 versus 5 cm, we expect a larger smoothing effect on the initial climate signal, which may incur much larger errors. In terms of site-specific validation of the bioturbation model, we note here that in the original publication of this data, the core consisted of fine, sub-millimeter scale laminations and was not bioturbated; thus, the application of the bioturbation is for demonstration only and actually oversmoothes the results relative to measurements. However, TURBO2 has been successfully used to simulate the impacts of bioturbation and improve model-data comparison in publications investigating both marine and lacustrine sites (e.g., Tierney et al., 2017; Thirumalai et al., 2018; Trauth, 1998, 2013).

Finally, we used Bchron to demonstrate the functionality of the observation submodel for Tanganyika. Figure 6 shows the series of calibrated radiocarbon dates (^{14}C) reported in Tierney et al. (2008; black triangles). The observation model yields an ensemble of 1,000 plausible chronologies (gray window) for a series of calibrated radiocarbon dates. Each of the 1,000 chronologies can be used to then quantify dating uncertainties across different horizons in the sediment core. For example, a user might extract the ensemble chronology data and test for maximum correlation with insolation or greenhouse gas forcing at a given site to isolate the age model ensemble member that maximizes agreement with climate forcing data or with other proximal paleoclimate records.

Figures 3–6 illustrate the utility of the submodel framework in the PSM through application to Lake Tanganyika. Each submodel (environment, sensor, archive, and observation) yields unique output, helping to quantify individual contributions of the full lake system to the final measured signal. For example, a user can quantify the change in measured climate variance from the original input signal to a signal that includes calibration uncertainties applied in the sensor model for GDGTs. This variance reduction could be subsequently compared to the change in variance in the proxy measurements due to bioturbation alone. While the uncertainty application occurs and is a part of the model output for each section of the lake model, the errors are additive and can be analyzed alone or en masse in the final output. In this way, the PSM submodels help identify where and how uncertainties are imparted and subsequently propagated through the PSM, filtering the input climate signal (Dee et al., 2015).

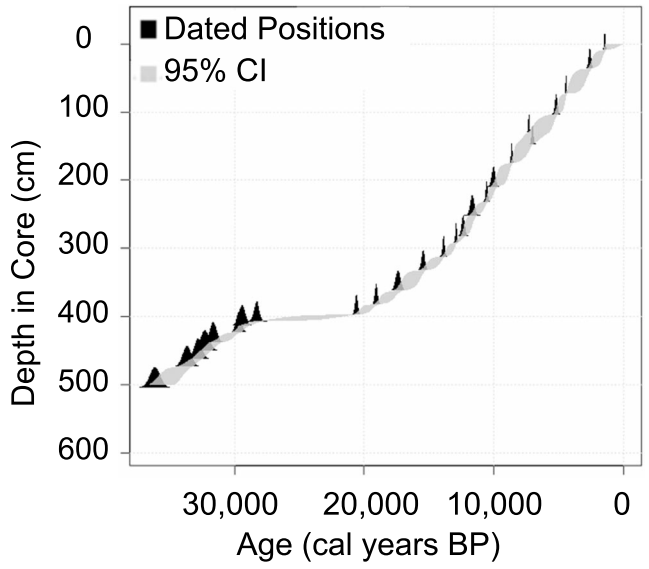

Figure 6. Observation model: BChron. Bchron-simulated chronologies (last glacial maximum–present) for Lake Tanganyika. The observation model yields an ensemble of 1,000 plausible chronologies (gray window) for a series of calibrated radiocarbon dates. The figure shows the output of Bchron using the C-14 ages and calibrations for Tanganyika TEX_{86} published in Tierney et al. (2008).

3.2. African Lake Temperatures During the LGM

Approximately 21,000 years ago, during the LGM, temperatures are estimated to have been between 3 and 5 °C colder globally as a result of low greenhouse gas concentrations (185 ppmv) and northern hemisphere ice sheet extent (Braconnot et al., 2012). The LGM thus provides an apt test bed for model simulations due to large and well-constrained temperature changes forced by greenhouse gas changes; it provides a different equilibrium climate state with which to compare model simulations (Hopcroft & Valdes, 2015). A number of proxy-model comparison studies have focused attention on the LGM (Braconnot et al., 2007; Chevalier et al., 2017; Harrison, 2000; Harrison et al., 2015; Pinot et al., 1999, and many others) but also on deeper time slices (e.g., the Miocene, Eocene, and Cretaceous; e.g., Huber & Caballero, 2011; Huber & Sloan, 2001; Poulsen et al., 1999, 2003; You et al., 2009). Such studies have compared temperature reconstructions, mostly derived from sea surface temperatures proxies and fossil leaves/pollen, to climate model simulations. In general, comparing available temperature reconstructions to climate model simulations with vastly different boundary conditions provides a unique test of model physics.

However, until recently, very few *temperature* reconstructions from tropical continents were available to assess model performance (Bartlein et al., 2011; Bonnefille et al., 1990; Chalie, 1995; Mark et al., 2005; Waelbroeck

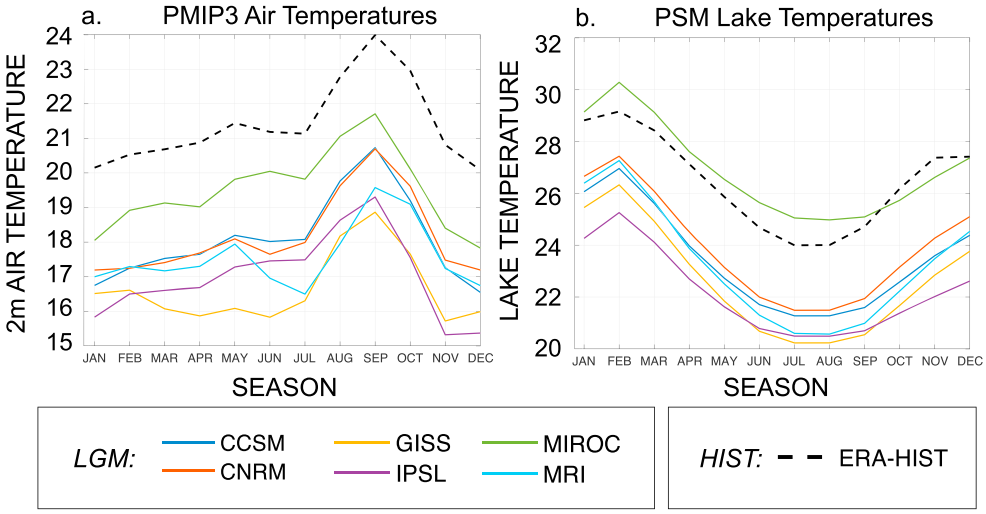

Figure 7. Air and lake surface temperatures at Lake Tanganyika, last glacial maximum (colored lines), and historical (black dotted line). (a) Simulated air temperature, climatological average, for six PMIP3 models with LGM simulations. (b) Simulated lake surface temperature, climatological averages, for 6 PMIP3 models with historical simulations. Using the PMIP3 air temperatures along with other environment model inputs, the lake proxy system model environment model simulates lake surface temperature climatologies at the last glacial maximum. The black-dotted line shows the comparison with historical (present day) temperatures, and each colored line represents a different PMIP3 model ensemble member. PMIP3 = Paleoclimate Modeling Intercomparison Project; PSM = proxy system model; LGM = last glacial maximum; HIST = historical.

et al., 2009). The recent application of GDGT-based analyses in tropical and subtropical lacustrine archives has changed that, adding much-needed data from the tropics to global databases of temperature changes from LGM to present (Loomis et al., 2011, 2017; Morrissey et al., 2018; Powers et al., 2005; Tierney et al., 2008). Complicating these data-model comparisons, however, is the fact that GDGT-based temperature proxies respond to lake (and *not* air) temperatures, creating uncertainty in the drivers of observed temperature changes and our methodology for assessing records alongside GCMs.

For example, recent analyses indicate that air-lake temperature relationships may be nonstationary (e.g., Hren & Sheldon, 2012; Kraemer et al., 2015) and depend on depth in the water column of GDGT production, both of which are poorly constrained in lacustrine environments. Kraemer et al. (2015) identified offsets between historical changes in lake surface temperature and TEX_{86} estimates in Lake Tanganyika and attribute the discrepancy to changes in mixed layer depth affecting GDGT producers at the thermocline. Yet sediment trap and water column analyses of GDGTs in Lake Tanganyika and Challa, East Africa, suggest that although production of GDGTs is the highest in the thermocline and hypolimnion, most sedimentary GDGTs are derived from production in the surface mixed layer and thermocline, due to packaging of GDGTs in rapidly sinking large sediment particles from grazing organisms (Buckles et al., 2014; Schouten et al., 2012). Further, in some cases, changing lake mixing can amplify air temperature changes, whereas in other lakes, temperatures may be damped compared to air temperature changes due to downward mixing of heat and the high specific heat capacity of water. These uncertainties motivate the following research questions: (1) are lake temperatures recording air temperature changes, and do lake and air temperatures differ in their relative means and patterns of change through time? and (2) is this relationship stationary?

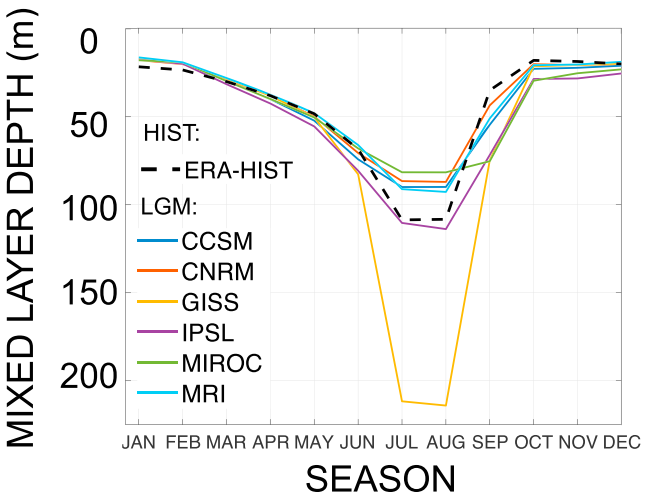

Figure 8. Simulated mixed layer depth, Lake Tanganyika, LGM, and historical. Simulated mixed layer depth (environment submodel), climatological average, for six PMIP3 models with LGM simulations compared to historical. The black-dotted line shows the comparison with historical (present day) temperatures, and each colored line represents a different PMIP3 model ensemble member. LGM =last glacial maximum.

Here we investigate changes in lake surface temperature, air temperature, and mixing depth in two lakes, Malawi and Tanganyika, from which the longest temperature records from the African continent have been pro-

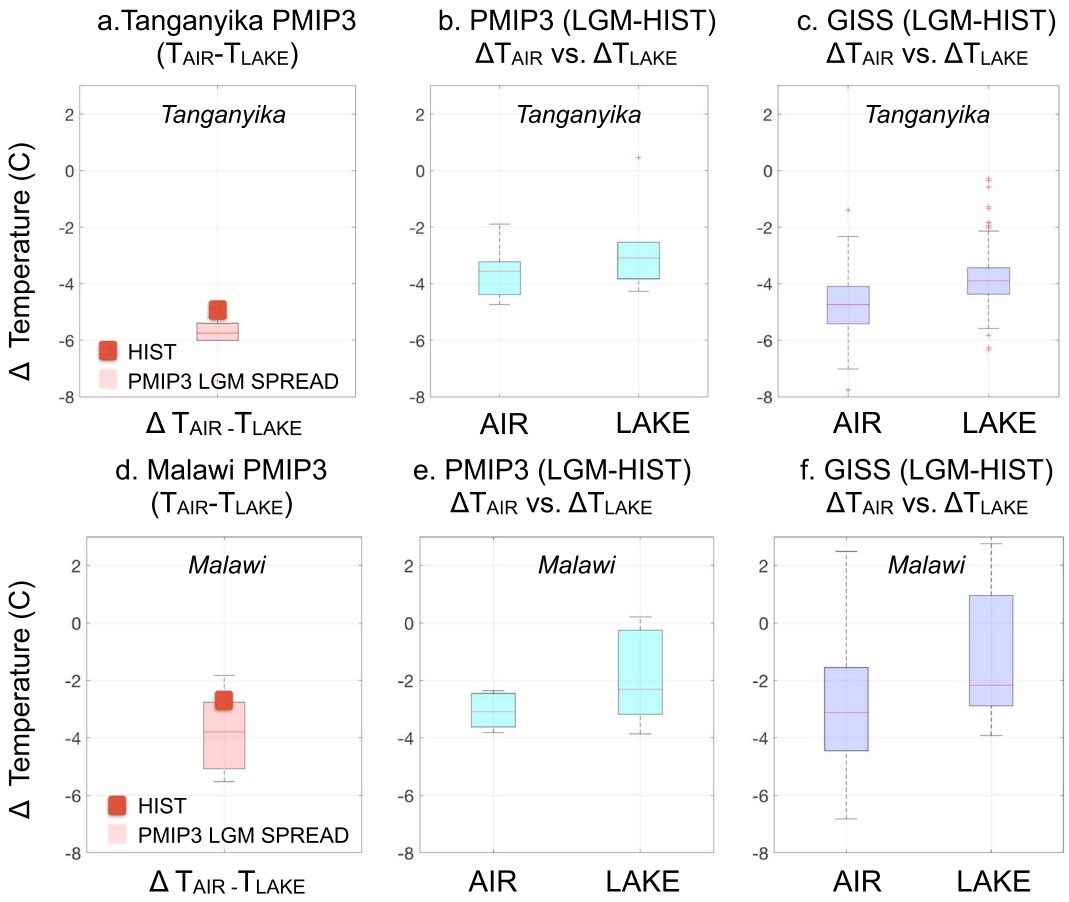

Figure 9. Differences in air temperatures and lake temperatures from the LGM to present, simulations for Tanganyika and Malawi. Tanganyika (a–c) and Malawi (d–f). (a and d) Differences between air and lake temperature through time: the red dot represents the mean value of the air-lake temperature difference over the historical period in ERA-Interim reanalysis and the resulting lake model simulation, and the box plots show the mean, interquartile range, and 95% confidence intervals for simulated temperatures. Each box plot shows shows the air-lake temperature difference for all of the PMIP3 model simulations at the LGM. This suggests the offset between lake and air temperatures is not stable in time. (b and e) LGM minus HIST difference in air and lake temperatures, PMIP3 model simulation spread represented by box plots. Lake temperature differences (LGM–present) are approximately 1 °C less than air temperature changes. (c and f) Same as (b) and (e) but for the GISS-PMIP3 LGM simulation only. $\Delta T_{AIR-LAKE}$ refers to the difference between lake and air temperatures in a given time slice (LGM, historical). $\Delta T - LAKE_{LGM-HIST}$ refers to the change in simulated lake surface temperatures, LGM minus historical. $\Delta T - AIR_{LGM-HIST}$ is the change in simulated air temperatures in PMIP3 models, LGM minus historical (note cooler temperatures at LGM in all cases). ΔT_{AIR} versus ΔT_{LAKE} is the difference between (LGM minus historical) temperature changes in simulated air temperatures compared to simulated changes in lake temperature. This value indicates that the absolute changes in air temperatures are offset from lake temperature changes by almost a degree. PMIP3 = Paleoclimate Modeling Intercomparison Project; LGM = last glacial maximum.

duced (Johnson et al., 2016; Powers et al., 2005; Tierney et al., 2008). The lake PSM allows us to explicitly link and test the impact of the lake system on modeled LGM temperatures, in particular to check whether lake temperatures and air temperature changes are comparable during the LGM and in the present. To date there has been little attempt to examine biases in the temperature proxies introduced by internal lake dynamics, in particular the energy transfers required to produce the observed temperature changes. As mentioned above, this is crucial as the proxy sensors modeled in this study are sensitive to lake temperature rather than the primary variable of interest: air temperature.

Our PSM environment model allows us to examine the surface energy fluxes that cause lake temperature variations in the past (e.g., latent heat losses related to humidity and winds, short and long wave radiation changes driven by orbital and greenhouse gas variation, and lake mixing). Importantly, we focus on output from the environment model only, given that the relationship in question is offsets between air temperature and lake temperature and the coevolution of those two variables. Since the conversion to proxy units uses a linear

Table 2
Results From LGM Lake and Air Temperature Application: Tanganyika and Malawi Lake Surface Temperatures Compared to Air Temperatures, LGM, and Historical

Temperature simulation/change	Tanganyika	Malawi
LGM $\Delta T_{AIR-LAKE}$ (C)	−5.9	−3.8
HIST $\Delta T_{AIR-LAKE}$ (C)	−5.0	−2.7
PMIP3 $\Delta T - LAKE_{LGM-HIST}$	−2.7	−1.9
PMIP3 $\Delta T - AIR_{LGM-HIST}$	−3.6	−3.1
GISS $\Delta T - LAKE_{LGM-HIST}$	−3.8	−0.97
GISS $\Delta T - AIR_{LGM-HIST}$	−4.7	−2.5
PMIP3 ΔT_{AIR} versus ΔT_{LAKE}	0.9	1.1
GISS ΔT_{AIR} versus ΔT_{LAKE}	0.9	1.5

Note. (top two rows) $\Delta T_{AIR-LAKE}$ refers to the difference between lake and air temperatures in a given time slice (LGM, historical). (middle four rows) $\Delta T - LAKE_{LGM-HIST}$ refers to the change in simulated lake surface temperatures, LGM minus historical. Similarly, $\Delta T - AIR_{LGM-HIST}$ is the change in simulated air temperatures in PMIP3 models, LGM minus historical (note cooler temperatures at LGM in all cases). Finally, the bottom two rows of the table show ΔT_{AIR} versus ΔT_{LAKE}, which is the difference between (LGM minus historical) temperature changes in simulated air temperatures compared to simulated changes in lake temperature. This value indicates that the absolute changes in air temperatures are offset from lake temperature changes by almost a degree. LGM = last glacial maximum; PMIP3 = Paleoclimate Modeling Intercomparison Project 3.

scaling, we do not expect the impacts of the sensor model will impact the result as strongly as lake surface energy balance. Further, because we are comparing average LGM time-slice values, we ignore impacts of sedimentation, bioturbation, and dating uncertainties, which likely impart uncertainty on shorter (multidecadal) timescales.

Simulated air temperatures and lake surface temperatures at the LGM compared to the historical period are shown in Figure 7. Figure 7a indicates GISS is the coldest model during the LGM at Tanganyika and MIROC the warmest. All models agree on the trends in the seasonal cycle for air temperatures, with hot JJASON temperatures and cooler DJFMAM temperatures. Interestingly, the sharp trends in the air temperature seasonal cycle are attenuated by the lake energy balance model (Figure 7b), such that warmest lake surface temperatures actually occur in NDJFM and coldest lake surface temperatures occur in JJAS. In agreement with previous studies, the energy balance model simulates maximum heat uptake in Tanganyika during SON (Tierney et al., 2011).

Evaluating the full PMIP3 model spread and resulting lake model simulations, a number of important observations arise. First, large changes in lake mixing depth during the LGM may partially account for differences in the amplitudes of LGM temperatures in proxy and model data. Figure 8 shows changes in the depth of the mixed layer at the LGM compared to historical simulations. While most of the PMIP3 simulations do not show a significant change in mixing depths, the coldest simulation in terms of both air temperature and lake surface temperatures (GISS, see orange line, Figure 7) shows a deepening of ~100 m. This is a large change, given the mean depth of the lake is 570 m. These changes in mixing depth (in GISS in particular) are partially driven by higher wind speed and reduced relative humidity at the lake surface, as lower humidity promotes higher rates of evaporation, evaporative cooling, and deeper mixing (see Figure 8).

Second, evaluation of lake surface temperatures and their relationship with model-simulated air temperature reveals nonstationarity in both (1) the air-lake temperature difference and (2) the change in air temperatures (LGM–present) versus the change in lake temperatures. Figure 9 shows changes for both Tanganyika (Figures 9a–9c) and Malawi (Figures 9d–9f), and these changes are summarized in Table 2. For (1), Figures 9a and 9d show that the differences between air and lake surface temperature for Tanganyika and Malawi exhibit larger offsets at the LGM (for Tanganyika, $T_{AIR-LAKE}$ = −5.6 to −7.5 °C) versus the historical period ($T_{AIR-LAKE}$ = −5.0 °C). For Lake Malawi, the offset is similar, and the air-lake offset is about 1° larger at the LGM. Lake temperatures are systematically warmer than air temperatures, similar to observations for Lakes

Tanganyika and Malawi (in agreement with, e.g., Kraemer et al., 2015; Tierney et al., 2008). Moreover, lake temperature proxy archives are sensitive to lake surface temperature changes, which are potentially damped by the lake system relative to air temperature change: Figures 9b and 9c show that $T_{AIR-LGM} - T_{AIR-HIST}$ in the PMIP3 ensemble differ by 0.9 °C, and looking at GISS alone (the coldest model simulation at the LGM), the difference in air temperature (LGM – present) is −5 °C. However, the total change in lake surface temperatures (LGM – present) is about a degree less (∼4 °C). Comparing these changes in absolute temperature to observations, GDGT-based reconstructions from Lake Tanganyika show a 4 °C warming from the LGM to preindustrial (22.5 to 26.5 °C; Powers et al., 2011). For Malawi, Figures 9e and 9f demonstrate similar trends to the Tanganyika data and show the lake system damping the total air temperature changes by approximately ∼1 °C. Our results suggest that the change in absolute temperature observed in lake surface temperature reconstructions is potentially damped compared to simulated (and actual) air temperature changes.

These tests highlight the importance of dynamical processes such as mixing in our interpretations of absolute temperature changes. Further, we note the potential complication that lake temperature proxies may have a nonstationary relationship with air temperature across large mean state changes in climate and, in general, may underestimate the air temperature change. However, this result is contingent on the selection of one of the more cold, dry, and windy PMIP3 simulations of the LGM (e.g., GISS).

4. Conclusions

Globally distributed lake temperature reconstructions provide crucial information relevant to climate prediction; such records yield statistics on the rates and magnitudes of temperature changes as recorded by paleoclimate archives, which inform our evaluation of temperature variability in models. However, paleoclimate archives often record climate in a multivariate and nonlinear manner, obfuscating the original climate variable of interest (e.g., temperature or precipitation). To this end, this work has developed a flexible, open-source PSM for lacustrine paleoclimate archives. The model includes an environment lake energy balance and vertical mixing model used to evaluate changes in lake temperature and mixing depth through time, as well as the fidelity of proxy estimates of air temperature versus lake surface temperature. It also simulates the response of various sensors in the lake, including δD of leaf waxes, carbonate $\delta^{18}O$, and GDGT-based temperature responses. Finally, the model explicitly simulates postdepositional processes that alter the final measured archive signal, including sedimentation, bioturbation, compaction, and uncertainties in the observation made on the measurement, including dating and analytical uncertainties.

Ultimately, the PSM output consists of a suite of pseudoproxy time series that first propagate uncertainty from the observed spread in GCM ensemble members through the lake temperature and mixing (environment) model. Mean annual lake surface temperature, season-specific lake temperatures, and lake temperatures at varying depths (with GCM ensemble spread) drive sensor, archive, and observation models, generating pseudoproxy time series that produce proxy calibration and analytical error, bioturbation, and compaction and age errors from an ensemble of plausible sediment core chronologies. All individual sources of uncertainty (lake-specific parameters, climate input fields, sediment processes, and age model uncertainties) ultimately compound and yield an uncertainty range in the final PSM output that allow for more robust comparisons with the lake temperature reconstructions in proxy units. Unique to the PSM framework, the individual contribution of each source of uncertainty can be tracked and quantified (section 3.1).

In addition, the lake PSM facilitates a robust characterization of the uncertainties applied to proxy measurements in a piecewise manner, such that the individual impacts of calibration uncertainty or age model error, for example, can be quantified. In future applications of this lake PSM, we hope to perform a more complete analysis of how uncertainties from each submodel (1) affect the input climate signal individually, but importantly, (2) interfere, whether constructively or destructively, with our interpretation of the variance contained in the input climate signal of interest.

The lake PSM thus improves our interpretation of past climate in lacustrine archives, helping users investigate the sensitivity of various proxy types to climatic changes. What percent change in precipitation is needed to simulate a 150-cm change in lake level over 100 years? How much do lake surface temperatures need to change to obtain a shift of 2% in carbonate $\delta^{18}O$? These and other questions are readily answered with the lake PSM presented in this work.

To demonstrate the utility of the lake PSM for advancing data-model comparisons, we investigated African temperature changes in current-generation PMIP3 simulations of the LGM and the historical period

(section 3.2). Environmental variables from PMIP3 simulations were used to drive the lake PSM at Malawi and Tanganyika to compare the behavior of means, seasonality, and depth variations in lake temperature and their relationship to air temperature over the 20th century using ERA-Interim Reanalysis products (Dee et al., 2011). These comparisons highlight confounding climatic influences on mixing depth and lake surface temperature, both which profoundly impact our understanding of how these lake systems respond to anthropogenic warming. We find that lake temperatures are damped compared to air temperatures and that there may be nonstationarity in mixing depths important for proxy interpretation. These results imply that lake temperature changes can originate from diverse forcings and that lake temperature changes may underestimate air temperature changes.

We acknowledge important limitations of this work. While we have attempted to create a model that is as adaptable and globally flexible as possible, the model does require many site-specific parameters and somewhat extensive user setup. The lake energy and water balance model in present form does not contain an example catchment model that would aid in the correct simulation of runoff, which may hinder users looking to accurately simulate changes in lake level; indeed, optimizing rainfall-runoff relationships and catchment models in this PSM framework represents a much needed realm of model development. One can imagine extensions of this publication of the PSM which incorporate options for more explicit catchment models (e.g., Barth et al., 2016; Matsubara & Howard, 2009). Alternatively, simplistic rainfall-runoff scaling relationship approaches (Budyko, 1961; Jakeman & Hornberger, 1993) may be appropriate (e.g., Ibarra et al., 2018; Quade et al., 2018).

While lake sediments incorporate a great number of sensors, here we have only built sensor submodels for three proxy types but hope to extend this functionality in the future, especially alongside forthcoming PSMs for marine sedimentary archives in R (e.g., Dolman & Laepple, 2018). Finally, meteorological and/or climate model data must be extracted for a given lake site to run the model; tools that facilitate extracting these variables are published alongside the PSM code to aid users in obtaining these data and formatting it to lake model input files.

Forthcoming work will seek to employ the full suite of updated PMIP4 simulations (Kageyama et al., 2018) to evaluate whether changes observed in the African temperature reconstructions are consistent across GCMs, time periods, and sites. We hope to further evaluate transient simulations of the last 21 ka against our reconstructions to determine the sensitivity of African temperatures to individual climate forcings.

This model is a first step toward the development and distribution of a publicly available, fully operational graphical user interface for lake sedimentary archives that will serve as a research tool for the paleoclimate community. The addition of the lake PSM to the `PRYSM` framework provides a new computational platform for the simulation of lake system archives and will establish standard practice for data-model comparison in the limnological community. We envision adapting this version of the model to facilitate advances in in situ and process-based studies involving lake systems and welcome contributions of additional sensor and archive models to this platform via a GitHub repository (https://github.com/sylvia-dee/PRYSM). Much progress has been made in the last several years in forward modeling for paleoclimatology to better understand archives, manage uncertainties, and make more robust comparisons with the dynamical information contained in state-of-the-art GCM simulations. We hope that this effort will stimulate collaborations between paleolimnologist data generators and climate modelers, jointly advancing knowledge of the drivers of major climate changes in the past and future.

Acknowledgments
This work was supported by the Peter Voss Postdoctoral Fellowship and the Institute at Brown for Environment and Society, the Brown University Department of Earth, Environmental, and Planetary Sciences, the Institute for Geophysics Postdoctoral Fellowship from the University of Texas at Austin, and the NOAA Climate Program Office. All of the code and input files used in this work can be found at https://github.com/sylvia-dee/PRYSM/. We thank Jesse Nusbaumer for providing precipitation isotope fields for the isotope-enabled component of the lake water balance model. The authors especially thank Jessica Tierney, Julien Emile-Geay, Bronwen Konecky, and Thomas Laepple for helpful conversations surrounding the development of this model. The authors also thank Daniel Ibarra and two anonymous reviewers for improving the quality of this work.

References

Anchukaitis, K. J., Evans, M. N., Kaplan, A., Vaganov, E. A., Hughes, M. K., Grissino-Mayer, H. D., & Cane, M. A. (2006). Forward modeling of regional scale tree-ring patterns in the southeastern United States and the recent influence of summer drought. *Geophysical Research Letters*, *33*, L04705. https://doi.org/:10.1029/2005GL025050

Bahr, D. B., Hutton, E. W., Syvitski, J. P., & Pratson, L. F. (2001). Exponential approximations to compacted sediment porosity profiles. *Computers & Geosciences*, *27*(6), 691–700.

Baker, A., Bradley, C., Phipps, S., Fischer, M., Fairchild, I., Fuller, L., et al. (2012). Millennial-length forward models and pseudoproxies of stalagmite δ^{18}O: An example from NW Scotland. *Climate of the Past*, *8*(4), 1153–1167.

Barth, C., Boyle, D. P., Hatchett, B. J., Bassett, S. D., Garner, C. B., & Adams, K. D. (2016). Late Pleistocene climate inferences from a water balance model of Jakes Valley, Nevada (USA). *Journal of paleolimnology*, *56*(2-3), 109–122.

Bartlein, P. J., Harrison, S. P., Brewer, S., Connor, S., Davis, B., Gajewski, K., et al. (2011). Pollen-based continental climate reconstructions at 6 and 21 ka: A global synthesis. *Climate Dynamics*, *37*(3-4), 775–802.

Bemis, B. E., Spero, H. J., Bijma, J., & Lea, D. W. (1998). Reevaluation of the oxygen isotopic composition of planktonic foraminifera: Experimental results and revised paleotemperature equations. *Paleoceanography*, *13*(2), 150–160.

Benson, L. (1994). Stable isotopes of oxygen and hydrogen in the Truckee River–Pyramid Lake surface-water column. 1. Data analysis and extraction of paleoclimatic information. *Limnology and oceanography*, *39*(2), 344–355.
Benson, L., & White, J. (1994). Stable isotopes of oxygen and hydrogen in the Truckee River–Pyramid Lake surface-water system. 3. Source of water vapor overlying pyramid lake. *Limnology and Oceanography*, *39*(8), 1945–1958.
Blaauw, M. (2010). Methods and code for 'classical' age-modelling of radiocarbon sequences. *Quaternary Geochronology*, *5*(5), 512–518. https://doi.org/10.1016/j.quageo.2010.01.002
Blaauw, M., & Christen, J. A. (2011). Flexible paleoclimate age-depth models using an autoregressive gamma process. *Bayesian Analysis*, *6*(3), 457–474.
Bonnefille, R., Roeland, J., & Guiot, J. (1990). Temperature and rainfall estimates for the past 40,000 years in equatorial Africa. *Nature*, *346*(6282), 347–349.
Bowen, G. J. (2009). The online isotopes in precipitation calculator, version 2.2. Retrieved from http://www. waterisotopes. org
Braconnot, P., Harrison, S. P., Kageyama, M., Bartlein, P. J., Masson-Delmotte, V., Abe-Ouchi, A., et al. (2012). Evaluation of climate models using palaeoclimatic data. *Nature Climate Change*, *2*(6), 417.
Braconnot, P., Otto-Bliesner, B., Harrison, S., Joussaume, S., Peterchmitt, J.-Y., Abe-Ouchi, A., et al. (2007). Results of PMIP2 coupled simulations of the Mid-Holocene and last glacial maximum—Part 1: Experiments and large-scale features. *Climate of the Past*, *3*(2), 261–277.
Breitenbach, S. F. M., Rehfeld, K., Goswami, B., Baldini, J. U. L., Ridley, H. E., Kennett, D. J., et al. (2012). COnstructing Proxy Records from Age models (COPRA). *Climate of the Past*, *8*, 1765–1779.
Bronk Ramsey, C. (1995). Radiocarbon calibration and analysis of stratigraphy: The OxCal program. *Radiocarbon*, *37*(2), 425–430.
Bronk-Ramsey, C. (2009). Bayesian analysis of radiocarbon dates. *Radiocarbon*, *51*(1), 337–360.
Buckles, L. K., Weijers, J. W., Verschuren, D., & Damsté, J. S. S. (2014). Sources of core and intact branched tetraether membrane lipids in the lacustrine environment: Anatomy of Lake Challa and its catchment, equatorial East Africa. *Geochimica et Cosmochimica Acta*, *140*, 106–126.
Budyko, M. I. (1961). The heat balance of the Earth's surface. *Soviet Geography*, *2*(4), 3–13.
Burgess, P. M., & Wright, V. P. (2003). Numerical forward modeling of carbonate platform dynamics: An evaluation of complexity and completeness in carbonate strata. *Journal of Sedimentary Research*, *73*(5), 637–652.
Chalie, F. (1995). Paleoclimates of the Southern Tanganyika Basin over the last 25-thousand years—Quantitative reconstruction from the statistical treatment of pollen data. *Comptes Rendus De L Academie Des Sciences Serie Ii*, *320*(3), 205–210.
Chevalier, M., Brewer, S., & Chase, B. M. (2017). Qualitative assessment of PMIP3 rainfall simulations across the Eastern African monsoon domains during the Mid-Holocene and the last glacial maximum. *Quaternary Science Reviews*, *156*, 107–120.
Costa, K., Russell, J., Konecky, B., & Lamb, H. (2014). Isotopic reconstruction of the African humid period and Congo air boundary migration at Lake Tana, Ethiopia. *Quaternary Science Reviews*, *83*, 58–67.
Crusius, J., & Anderson, R. F. (1991). Core compression and surficial sediment loss of lake sediments of high porosity caused by gravity coring. *Limnology and Oceanography*, *36*(5), 1021–1030.
De Jonge, C., Hopmans, E. C., Zell, C. I., Kim, J.-H., Schouten, S., & Damsté, J. S. S. (2014). Occurrence and abundance of 6-methyl branched glycerol dialkyl glycerol tetraethers in soils: Implications for palaeoclimate reconstruction. *Geochimica et Cosmochimica Acta*, *141*, 97–112.
Dean, J. R., Jones, M. D., Leng, M. J., Metcalfe, S. E., Sloane, H. J., Eastwood, W. J., & Roberts, C. N. (2018). Seasonality of holocene hydroclimate in the Eastern Mediterranean reconstructed using the oxygen isotope composition of carbonates and diatoms from Lake Nar, Central Turkey. *The Holocene*, *28*(2), 267–276.
Dee, S., Emile-Geay, J., Evans, M., Allam, A., Steig, E., & Thompson, D. (2015). Prysm: An open-source framework for proxy system modeling, with applications to oxygen-isotope systems. *Journal of Advances in Modeling Earth Systems*, *7*, 1220–1247.
Dee, S., Parsons, L., Loope, G., Overpeck, J., Ault, T., & Emile-Geay, J. (2017). Improved spectral comparisons of paleoclimate models and observations via proxy system modeling: Implications for multi-decadal variability. *Earth and Planetary Science Letters*, *476*, 34–46.
Dee, S. G., Steiger, N. J., Emile-Geay, J., & Hakim, G. J. (2016). On the utility of proxy system models for estimating climate states over the common era. *Journal of Advances in Modeling Earth Systems*, *8*, 1164–1179.
Dee, D., Uppala, S., Simmons, A., Berrisford, P., Poli, P., Kobayashi, S., et al. (2011). The ERA-Interim reanalysis: Configuration and performance of the data assimilation system. *Quarterly Journal of the Royal Meteorological Society*, *137*(656), 553–597.
Descy, J., Plisnier, P., Leporcq, B., Sténuite, S., Pirlot, S., Stimart, J., et al. (2006). *Climate variability as recorded in Lake Tanganyika (CLIMLAKE)*. Brussels: Belgian science Policy.
Dolman, A. M., & Laepple, T. (2018). Sedproxy: a forward model for sediment archived climate proxies. *Climate of the Past Discussions*, 1–31. https://doi.org/10.5194/cp-2018-13
Erez, J., & Luz, B. (1983). Experimental paleotemperature equation for planktonic foraminifera. *Geochimica et Cosmochimica Acta*, *47*(6), 1025–1031.
Evans, M. N., Tolwinski-Ward, S. E., Thompson, D. M., & Anchukaitis, K. J. (2013). Applications of proxy system modeling in high resolution paleoclimatology. *Quaternary Science Reviews*, *76*(0), 16–28. https://doi.org/10.1016/j.quascirev.2013.05.024
Feakins, S. J., Kirby, M. E., Cheetham, M. I., Ibarra, Y., & Zimmerman, S. R. (2014). Fluctuation in leaf wax D/H ratio from a southern California lake records significant variability in isotopes in precipitation during the late Holocene. *Organic Geochemistry*, *66*, 48–59.
Garratt, J. (1977). Review of drag coefficients over oceans and continents. *Monthly Weather Review*, *105*(7), 915–929.
Gasse, F. (2000). Hydrological changes in the African tropics since the last glacial maximum. *Quaternary Science Reviews*, *19*(1), 189–211.
Harrison, S. P. (2000). Palaeoenvironmental data sets and model evaluation in PMIP. In *Proceedings of the Third PMIP Workshop, Canada*. WCRP-111, WMO/TD-No. 1007., 4th - 8th October 1999., Canada (pp. 25–42). Geneva, Switzerland: WORLD METEOROLOGICAL ORGANIZATION-PUBLICATIONS-WMO TD.
Harrison, S. P., Bartlein, P., Izumi, K., Li, G., Annan, J., Hargreaves, J., et al. (2015). Evaluation of CMIP5 palaeo-simulations to improve climate projections. *Nature Climate Change*, *5*(8), 735.
Harrison, S. P., Bartlein, P. J., & Prentice, I. C. (2016). What have we learnt from palaeoclimate simulations? *Journal of Quaternary Science*, *31*(4), 363–385.
Haslett, J., & Parnell, A. (2008). A simple monotone process with application to radiocarbon-dated depth chronologies. *Journal of the Royal Statistical Society: Series C (Applied Statistics)*, *57*(4), 399–418.
Hopcroft, P. O., & Valdes, P. J. (2015). Last glacial maximum constraints on the Earth System model HadGEM2-ES. *Climate Dynamics*, *45*(5-6), 1657–1672.
Hostetler, S. (1991). Simulation of lake ice and its effect on the late-Pleistocene evaporation rate of Lake Lahontan. *Climate Dynamics*, *6*(1), 43–48.

Hostetler, S. (2009). Use of models and observations to assess trends in the 1950–2005 water balance and climate of Upper Klamath Lake, Oregon. *Water resources research*, *45*, W12409. https://doi.org/10.1029/2008WR007295

Hostetler, S., & Bartlein, P. (1990). Simulation of lake evaporation with application to modeling lake level variations of Harney-Malheur Lake, Oregon. *Water Resources Research*, *26*(10), 2603–2612.

Hostetler, S., & Benson, L. (1994). Stable isotopes of oxygen and hydrogen in the Truckee River–Pyramid Lake surface-water system. 2. A predictive model of δ^{18}O and 18^2H in Pyramid Lake. *Limnology and Oceanography*, *39*(2), 356–364.

Hostetler, S., & Benson, L. (1994). Stable isotopes of oxygen and hydrogen in the Truckee River–Pyramid Lake surface-water system. 2. A predictive model of δ^{18}O and 18^2H in Pyramid Lake. *Limnology and Oceanography*, *39*(2), 356–364.

Hren, M. T., & Sheldon, N. D. (2012). Temporal variations in lake water temperature: Paleoenvironmental implications of lake carbonate δ^{18}O and temperature records. *Earth and Planetary Science Letters*, *337*, 77–84.

Huber, M., & Caballero, R. (2011). The early Eocene equable climate problem revisited. *Climate of the Past*, *7*, 603–633. https://doi.org/10.5194/cp-7-603-2011

Huber, M., & Sloan, L. C. (2001). Heat transport, deep waters, and thermal gradients: Coupled simulation of an Eocene greenhouse climate. *Geophysical Research Letters*, *28*(18), 3481–3484.

Huybers, P., & Wunsch, C. (2004). A depth-derived Pleistocene age model: Uncertainty estimates, sedimentation variability, and nonlinear climate change. *Paleoceanography*, *19*, PA1028. https://doi.org/10.1029/2002PA000857

IAEA/WMO (2014). Global network of isotopes in precipitation. GNIP database.

IPCC (2013). *Summary for policymakers, book section SPM* (pp. 1–30). Cambridge, UK and New York: Cambridge University Press. https://doi.org/10.1017/CBO9781107415324.004

Ibarra, D. E., Oster, J. L., Winnick, M. J., Caves Rugenstein, J. K., Byrne, M. P., & Chamberlain, C. P. (2018). Warm and cold wet states in the western United States during the Pliocene–Pleistocene. *Geology*, *46*(4), 355–358.

Jakeman, A., & Hornberger, G. (1993). How much complexity is warranted in a rainfall-runoff model? *Water Resources Research*, *29*(8), 2637–2649.

Johnson, T., Werne, J., Brown, E., Abbott, A., Berke, M., Steinman, B., et al. (2016). A progressively wetter climate in southern East Africa over the past 1.3 million years. *Nature*, *537*(7619), 220.

Jones, M. D., Cuthbert, M. O., Leng, M. J., McGowan, S., Mariethoz, G., Arrowsmith, C., et al. (2016). Comparisons of observed and modelled lake δ^{18}O variability. *Quaternary Science Reviews*, *131*, 329–340.

Jones, M. D., Leng, M. J., Roberts, C. N., Türkeş, M., & Moyeed, R. (2005). A coupled calibration and modelling approach to the understanding of dry-land lake oxygen isotope records. *Journal of Paleolimnology*, *34*(3), 391–411.

Kageyama, M., Braconnot, P., Harrison, S. P., Haywood, A. M., Jungclaus, J., Otto-Bliesner, B. L., et al. (2018). PMIP4-CMIP6: the contribution of the Paleoclimate Modelling Intercomparison Project to CMIP6. *Geoscientific Model Development Discussions*, *11*(3), 1033–1057.

Kim, S.-T., & O'Neil, J. R. (1997). Equilibrium and nonequilibrium oxygen isotope effects in synthetic carbonates. *Geochimica et Cosmochimica Acta*, *61*(16), 3461–3475.

Klauenberg, K., Blackwell, P. G., Buck, C. E., Mulvaney, R., Röthlisberger, R., & Wolff, E. W. (2011). Bayesian glaciological modelling to quantify uncertainties in ice core chronologies. *Quaternary Science Reviews*, *30*(21), 2961–2975.

Konecky, B., Russell, J., & Bijaksana, S. (2016). Glacial aridity in central Indonesia coeval with intensified monsoon circulation. *Earth and Planetary Science Letters*, *437*, 15–24.

Konecky, B. L., Russell, J. M., Johnson, T. C., Brown, E. T., Berke, M. A., Werne, J. P., & Huang, Y. (2011). Atmospheric circulation patterns during late Pleistocene climate changes at Lake Malawi, Africa. *Earth and Planetary Science Letters*, *312*(3), 318–326.

Kraemer, B. M., Hook, S., Huttula, T., Kotilainen, P., O'Reilly, C. M., Peltonen, A., et al. (2015). Century-long warming trends in the upper water column of Lake Tanganyika. *PLoS One*, *10*(7), e0132490.

Kutzbach, J. E., & Street-Perrott, F. A. (1985). Milankovitch forcing of fluctuations in the level of tropical lakes from 18 to 0 kyr BP. *Nature*, *317*(6033), 130–134.

Laepple, T., & Huybers, P. (2014). Global and regional variability in marine surface temperatures. *Geophysical Research Letters*, *41*, 2528–2534. https://doi.org/10.1002/2014GL059345

Leng, M. J., & Marshall, J. D. (2004). Palaeoclimate interpretation of stable isotope data from lake sediment archives. *Quaternary Science Reviews*, *23*(7-8), 811–831.

Li, Y., & Morrill, C. (2013). Lake levels in Asia at the last glacial maximum as indicators of hydrologic sensitivity to greenhouse gas concentrations. *Quaternary Science Reviews*, *60*, 1–12.

Loomis, S. E., Russell, J. M., & Damsté, J. S. S. (2011). Distributions of branched GDGTs in soils and lake sediments from Western Uganda: Implications for a lacustrine paleothermometer. *Organic Geochemistry*, *42*(7), 739–751.

Loomis, S. E., Russell, J. M., Ladd, B., Street-Perrott, F. A., & Damsté, J. S. S. (2012). Calibration and application of the branched GDGT temperature proxy on East African lake sediments. *Earth and Planetary Science Letters*, *357*, 277–288.

Loomis, S. E., Russell, J. M., Verschuren, D., Morrill, C., De Cort, G., Damsté, J. S. S., et al. (2017). The tropical lapse rate steepened during the last glacial maximum. *Science Advances*, *3*(1), e1600815.

Lorenz, D. J., Nieto-Lugilde, D., Blois, J. L., Fitzpatrick, M. C., & Williams, J. W. (2016). Downscaled and debiased climate simulations for North America from 21,000 years ago to 2100AD. *Scientific Data*, *3*, 160048.

Lou, J., Schwab, D. J., Beletsky, D., & Hawley, N. (2000). A model of sediment resuspension and transport dynamics in southern Lake Michigan. *Journal of Geophysical Research*, *105*(C3), 6591–6610.

Lowry, D. P., & Morrill, C. (2018). Is the last glacial maximum a reverse analog for future hydroclimate changes in the Americas? *Climate Dynamics*, 1–21. https://doi.org/10.1007/s00382-018-4385-y

Mark, B., Harrison, S., Spessa, A., New, M., Evans, D., & Helmens, K. (2005). Tropical snowline changes at the last glacial maximum: A global assessment. *Quaternary International*, *138*, 168–201.

Matsubara, Y., & Howard, A. D. (2009). A spatially explicit model of runoff, evaporation, and lake extent: Application to modern and late Pleistocene lakes in the Great Basin region, western United States. *Water Resources Research*, *45*, W06425. https://doi.org/10.1029/2007WR005953

Meinshausen, M., Smith, S. J., Calvin, K., Daniel, J. S., Kainuma, M. L. T., Lamarque, J. F., et al. (2011). The Paleoclimate Modeling Intercomparison Project contribution to CMIP5. WCRP Coupled Model Intercomparison Project-Phase 5-CMIP5 (15 pp.).

Morrill, C., Small, E. E., & Sloan, L. C. (2001). Modeling orbital forcing of lake level change: Lake Gosiute (Eocene), North America. *Global and Planetary Change*, *29*(1), 57–76.

Morrissey, A., Scholz, C. A., & Russell, J. M. (2018). Late Quaternary TEX_{86} paleotemperatures from the world's largest desert lake, Lake Turkana, Kenya. *Journal of Paleolimnology*, *59*(1), 103–117.

Nusbaumer, J., Wong, T. E., Bardeen, C., & Noone, D. (2017). Evaluating hydrological processes in the Community Atmosphere Model version 5 (CAM5) using stable isotope ratios of water. *Journal of Advances in Modeling Earth Systems*, *9*, 949–977.

O'Neil, J. R., Clayton, R. N., & Mayeda, T. K. (1969). Oxygen isotope fractionation in divalent metal carbonates. *The Journal of Chemical Physics*, *51*(12), 5547–5558.

O'reilly, C. M., Alin, S. R., Plisnier, P.-D., Cohen, A. S., & McKee, B. A. (2003). Climate change decreases aquatic ecosystem productivity of Lake Tanganyika, Africa. *Nature*, *424*(6950), 766–768.

Otto-Bliesner, B. L., Russell, J. M., Clark, P. U., Liu, Z., Overpeck, J. T., Konecky, B., et al. (2014). Coherent changes of southeastern equatorial and northern African rainfall during the last deglaciation. *Science*, *346*(6214), 1223–1227.

Parnell, A. C., Buck, C. E., & Doan, T. K. (2011). A review of statistical chronology models for high-resolution, proxy-based Holocene palaeoenvironmental reconstruction. *Quaternary Science Reviews*, *30*(21), 2948–2960. https://doi.org/10.1016/j.quascirev.2011.07.024

Patterson, J., & Hamblin, P. (1988). Thermal simulation of a lake with winter ice cover. *Limnology and Oceanography*, *33*(3), 323–338.

Pinot, S., Ramstein, G., Harrison, S., Prentice, I., Guiot, J., Stute, M., & Joussaume, S. (1999). Tropical paleoclimates at the last glacial maximum: Comparison of Paleoclimate Modeling Intercomparison Project (PMIP) simulations and paleodata. *Climate Dynamics*, *15*(11), 857–874.

Plisnier, P.-D., Chitamwebwa, D., Mwape, L., Tshibangu, K., Langenberg, V., & Coenen, E. (1999). Limnological annual cycle inferred from physical-chemical fluctuations at three stations of Lake Tanganyika. In O. V. Lindqvist, H. Mölsä, K. Salonen, & J. Sarvala (Eds.), *From limnology to fisheries: Lake Tanganyika and other large lakes* (pp. 45–58). Dordrecht, The Netherlands: Springer.

Poulsen, C. J., Barron, E. J., Peterson, W. H., & Wilson, P. A. (1999). A reinterpretation of mid-Cretaceous shallow marine temperatures through model-data comparison. *Paleoceanography*, *14*(6), 679–697.

Poulsen, C. J., Gendaszek, A. S., & Jacob, R. L. (2003). Did the rifting of the Atlantic Ocean cause the Cretaceous thermal maximum? *Geology*, *31*(2), 115–118.

Powers, L. A., Johnson, T. C., Werne, J. P., Castañeda, I. S., Hopmans, E. C., Damsté, J. S. S., & Schouten, S. (2011). Organic geochemical records of environmental variability in Lake Malawi during the last 700 years, part I: The TEX_{86} temperature record. *Palaeogeography, Palaeoclimatology, Palaeoecology*, *303*(1), 133–139.

Powers, L. A., Johnson, T. C., Werne, J. P., Castaneda, I. S., Hopmans, E. C., Sinninghe Damsté, J. S., & Schouten, S. (2005). Large temperature variability in the southern African tropics since the last glacial maximum. *Geophysical Research Letters*, *32*, L08706. https://doi.org/10.1029/2004GL022014

Powers, L., Werne, J. P., Vanderwoude, A. J., Damsté, J. S. S., Hopmans, E. C., & Schouten, S. (2010). Applicability and calibration of the TEX_{86} paleothermometer in lakes. *Organic Geochemistry*, *41*(4), 404–413.

Quade, J., Dente, E., Armon, M., Dor, Y. B., Morin, E., Adam, O., & Enzel, Y. (2018). Megalakes in the Sahara? A review. *Quaternary Research*, *90*, 253–275. https://doi.org/10.1017/qua.2018.46

Ramsey, C. B. (2008). Deposition models for chronological records. *Quaternary Science Reviews*, *27*(1), 42–60.

Russell, J. M., Hopmans, E. C., Loomis, S. E., Liang, J., & Damsté, J. S. S. (2018). Distributions of 5-and 6-methyl branched glycerol dialkyl glycerol tetraethers (brGDGTs) in East African lake sediment: Effects of temperature, pH, and new lacustrine paleotemperature calibrations. *Organic Geochemistry*, *117*, 56–69.

Russell, J. M., McCoy, S., Verschuren, D., Bessems, I., & Huang, Y. (2009). Human impacts, climate change, and aquatic ecosystem response during the past 2000 yr at Lake Wandakara, Uganda. *Quaternary Research*, *72*(3), 315–324.

Russell, J. M., Vogel, H., Konecky, B. L., Bijaksana, S., Huang, Y., Melles, M., et al. (2014). Glacial forcing of central Indonesian hydroclimate since 60,000 y BP. *Proceedings of the National Academy of Sciences*, *111*(14), 5100–5105.

Russon, T., Tudhope, A. W., Hegerl, G. C., Collins, M., & Tindall, J. (2013). Inter-annual tropical Pacific climate variability in an isotope-enabled CGCM: Implications for interpreting coral stable oxygen isotope records of ENSO. *Climate of the Past*, *9*(4), 1543–1557. https://doi.org/10.5194/cp-9-1543-2013

Sachse, D., Billault, I., Bowen, G. J., Chikaraishi, Y., Dawson, T. E., Feakins, S. J., et al. (2012). Molecular paleohydrology: Interpreting the hydrogen-isotopic composition of lipid biomarkers from photosynthesizing organisms. *Annual Review of Earth and Planetary Sciences*, *40*, 221–249.

Schmidt, G. A. (1999). Forward modeling of carbonate proxy data from planktonic foraminifera using oxygen isotope tracers in a global ocean model. *Paleoceanography*, *14*(4), 482–497.

Schouten, S., Hopmans, E. C., Schefuß, E., & Damste, J. S. S. (2002). Distributional variations in marine crenarchaeotal membrane lipids: A new tool for reconstructing ancient sea water temperatures? *Earth and Planetary Science Letters*, *204*(1-2), 265–274.

Schouten, S., Rijpstra, W. I. C., Durisch-Kaiser, E., Schubert, C. J., & Damsté, J. S. S. (2012). Distribution of glycerol dialkyl glycerol tetraether lipids in the water column of Lake Tanganyika. *Organic Geochemistry*, *53*, 34–37.

Small, E. E., Sloan, L. C., Hostetler, S., & Giorgi, F. (1999). Simulating the water balance of the aral sea with a coupled regional climate-lake model. *Journal of Geophysical Research*, *104*(D6), 6583–6602.

Steig, E. J., Ding, Q., White, J. W., Küttel, M., Rupper, S. B., Neumann, T. A., et al. (2013). Recent climate and ice-sheet changes in West Antarctica compared with the past 2,000 years. *Nature Geoscience*, *6*(5), 372–375.

Steiger, N. J., Hakim, G. J., Steig, E. J., Battisti, D. S., & Roe, G. H. (2014). Assimilation of time-averaged pseudoproxies for climate reconstruction. *Journal of Climate*, *27*(1), 426–441.

Steinman, B. A., Abbott, M. B., Nelson, D. B., Stansell, N. D., Finney, B. P., Bain, D. J., & Rosenmeier, M. F. (2013). Isotopic and hydrologic responses of small, closed lakes to climate variability: Comparison of measured and modeled lake level and sediment core oxygen isotope records. *Geochimica et Cosmochimica Acta*, *105*, 455–471.

Stoll, H. M., Müller, W., & Prieto, M. (2012). I-STAL, a model for interpretation of Mg/Ca, Sr/Ca and Ba/Ca variations in speleothems and its forward and inverse application on seasonal to millennial scales. *Geochemistry, Geophysics, Geosystems*, *13*, Q09004. https://doi.org/10.1029/2012GC004183

Street-Perrott, F. A. (1994). Palaeo-perspectives: Changes in terrestrial ecosystems. *Ambio*, *23*, 37–43.

Subin, Z. M., Riley, W. J., & Mironov, D. (2012). An improved lake model for climate simulations: Model structure, evaluation, and sensitivity analyses in CESM1. *Journal of Advances in Modeling Earth Systems*, *4*, M02001. https://doi.org/10.1029/2011MS000072

Thirumalai, K., Quinn, T. M., Okumura, Y., Richey, J. N., Partin, J. W., Poore, R. Z., & Moreno-Chamarro, E. (2018). Pronounced centennial-scale Atlantic Ocean climate variability correlated with Western Hemisphere hydroclimate. *Nature Communications*, *9*(1), 392.

Thompson, D. M., Ault, T. R., Evans, M. N., Cole, J. E., & Emile-Geay, J. (2011). Comparison of observed and simulated tropical climate trends using a forward model of coral $\delta^{18}O$. *Geophysical Research Letters*, *38*, L14706. https://doi.org/10.1029/2011GL048224

Tierney, J. E., Lewis, S. C., Cook, B. I., LeGrande, A. N., & Schmidt, G. A. (2011). Model, proxy and isotopic perspectives on the East African humid period. *Earth and Planetary Science Letters*, *307*(1), 103–112.

Tierney, J. E., Oppo, D. W., Rosenthal, Y., Russell, J. M., & Linsley, B. K. (2010). Coordinated hydrological regimes in the Indo-Pacific region during the past two millennia. *Paleoceanography*, *25*, PA1102. https://doi.org/10.1029/2009PA001871

Tierney, J. E., Pausata, F. S., & deMenocal, P. B. (2017). Rainfall regimes of the Green Sahara. *Science Advances*, *3*(1), e1601503.

Tierney, J. E., Russell, J. M., & Huang, Y. (2010). A molecular perspective on Late Quaternary climate and vegetation change in the Lake Tanganyika basin, East Africa. *Quaternary Science Reviews*, *29*(5), 787–800.

Tierney, J. E., Mayes, M. T., Meyer, N., Johnson, C., Swarzenski, P. W., Cohen, A. S., & Russell, J. M. (2010). Late-twentieth-century warming in Lake Tanganyika unprecedented since AD 500. *Nature Geoscience*, *3*(6), 422.

Tierney, J. E., Russell, J. M., Huang, Y., Damsté, J. S. S., Hopmans, E. C., & Cohen, A. S. (2008). Northern Hemisphere controls on tropical southeast African climate during the past 60,000 years. *Science*, *322*(5899), 252–255.

Tierney, J. E., & Tingley, M. P. (2015). A TEX_{86} surface sediment database and extended Bayesian calibration. *Scientific Data*, *2*, 150029.

Trauth, M. H. (1998). TURBO: A dynamic-probabilistic simulation to study the effects of bioturbation on paleoceanographic time series. *Computers & Geosciences*, *24*(5), 433–441.

Trauth, M. H. (2013). TURBO2: A matlab simulation to study the effects of bioturbation on paleoceanographic time series. *Computers & Geosciences*, *61*, 1–10.

Vassiljev, J., Harrison, S. P., & Guiot, J. (1998). Simulating the Holocene lake-level record of Lake Bysjön, southern Sweden. *Quaternary Research*, *49*(1), 62–71.

Verburg, P., & Hecky, R. E. (2003). Wind patterns, evaporation, and related physical variables in Lake Tanganyika, East Africa. *Journal of Great Lakes Research*, *29*, 48–61.

Viau, A., & Gajewski, K. (2001). Holocene variations in the global hydrological cycle quantified by objective gridding of lake level databases. *Journal of Geophysical Research*, *106*(D23), 31703–31716.

Wackerbarth, A., Langebroek, P., Werner, M., Lohmann, G., Riechelmann, S., Borsato, A., & Mangini, A. (2012). Simulated oxygen isotopes in cave drip water and speleothem calcite in European caves. *Climate of the Past*, *8*(6), 1781–1799.

Waelbroeck, C., Paul, A., Kucera, M., Rosell-Melé, A., Weinelt, M., Schneider, R., et al. (2009). Constraints on the magnitude and patterns of ocean cooling at the last glacial maximum. *Nature Geoscience*, *2*(2), 127.

Weijers, J. W., Schouten, S., van den Donker, J. C., Hopmans, E. C., & Damsté, J. S. S. (2007). Environmental controls on bacterial tetraether membrane lipid distribution in soils. *Geochimica et Cosmochimica Acta*, *71*(3), 703–713.

You, Y., Huber, M., Müller, R., Poulsen, C., & Ribbe, J. (2009). Simulation of the middle Miocene climate optimum. *Geophysical Research Letters*, *36*, L04702. https://doi.org/10.1029/2008GL036571